Increased misfolding and truncation of tau in APP/PS1/tau transgenic mice compared to mutant tau mice

[1]Céline Héraud, [1]Doris Goufak, [1]Kunie Ando, [1]Karelle Leroy, [1]Valérie Suain, [1]Zehra Yilmaz, [1]Robert De Decker, [1]Michèle Authelet, [2]Vincent Laporte, [2]Jean-Noël Octave, [1]Jean-Pierre Brion.

[1]Université Libre de Bruxelles (ULB), Laboratory of Histology, Neuroanatomy and Neuropathology, ULB Neuroscience Institute, B-1070 Brussels, Belgium.
[2]Université Catholique de Louvain (UCL), Institute of Neuroscience, B-1200 Brussels, Belgium

Abbreviated title: Enhanced tau misfolding in APP/PS1/tau mice

Send correspondence to:
Dr Jean-Pierre Brion
Université Libre de Bruxelles (ULB), Faculty of Medicine. Laboratory of Histology, Neuroanatomy and Neuropathology.
808, route de Lennik, Bldg GE
1070 – Brussels, BELGIUM
Tel: 32 - 2 – 5556505. Fax: 32 - 2 – 5556285. E-mail: jpbrion@ulb.ac.be

Neurobiology of Disease (2013) 62C: 100-112
Doi 10.1016/j.nbd.2013.09.010

Abstract

Neurofibrillary degeneration in transgenic models of tauopathies has been observed to be enhanced when these models are crossed with transgenic models developing an Aß pathology. The mechanisms leading to this enhanced tau pathology are not well understood. We have performed a detailed analysis of tau misprocessing in a new transgenic mouse model combining APP, PS1 and tau mutations (5xFAD x Tg30 mice) by comparison with littermates expressing only a FTD mutant tau (Tg30 mice). These 5xFAD x Tg30 mice showed a more severe deficient motor phenotype than Tg30 mice and developed with age a dramatically accelerated NFT load in brain compared to Tg30 mice. Insoluble tau in 5xFAD x Tg30 mice compared to insoluble tau in Tg30 mice showed increased phosphorylation, enhanced misfolding and truncation changes mimicking more closely the post-translational changes characteristic of PHF-tau in Alzheimer's disease. Endogenous wild-type mouse tau was recruited at much higher levels in insoluble tau in 5xFAD x Tg30 than in Tg30 mice. Extracellular amyloid load, Aß40 and Aß42, ß-CTFs and ß-CTFs phosphorylation levels were lower in 5xFAD x Tg30 mice than in 5xFAD mice. Despite this reduction of Aß, a significant hippocampal neuronal loss was observed in 5xFAD x Tg30 but not in 5xFAD mice indicating its closer association with increased tau pathology. This 5xFAD x Tg30 model thus mimics more faithfully tau pathology and neuronal loss observed in AD and suggests that additional post-translational changes in tau and self-recruitment of endogenous tau drive the enhanced tau pathology developing in presence of Aß pathology.

Key words: tau; APP; PS1; neurofibrillary tangles; Aß; Alzheimer; transgenic

1. Introduction

Sporadic and familial forms of Alzheimer's disease (AD) due to mutations in the presenilins (PS) and the amyloid precursor protein (APP) genes are neuropathologically characterized by the presence of both neurofibrillary tangles (NFT) and senile plaques. NFT are made of bundles of paired helical filaments (PHF) composed of the microtubule-associated protein tau (Brion et al., 1985). PHF are composed of modified tau (PHF-tau) proteins that are hyperphosphorylated and abnormally phosphorylated (Grundke-Iqbal et al., 1986), conformationnaly altered, and truncated (Buée et al., 2000). Senile plaques are complex structures made of an extracellular core of amyloid surrounded by dystrophic neurites and reactive glial cells. The amyloid core is mainly composed of the Aß peptide derived from proteolytic cleavage of APP. According to the amyloid cascade hypothesis, the formation of the Aß peptide is an upstream event inducing tau phosphorylation, tau aggregation and NFT formation (Hardy and Selkoe, 2002). However, transgenic mice overexpressing mutated APP and/or PS1 gene(s) do not develop NFT, even when they also express a human wild-type tau protein (Boutajangout et al., 2004). Conversely, transgenic mice expressing an FTD mutant tau develop NFT but not amyloid plaques. Several studies in animal models have nevertheless indicated that Aß can increase tau pathology in transgenic mice expressing a FTD mutant tau. Injection of Aß (Gotz et al., 2001) or of Aβ-containing brain extract from APP mice (Bolmont et al., 2007) was reported to increase NFT formation in mutant P301L tau mice. Double transgenic mice expressing mutants APP and tau proteins develop an enhanced tau pathology (Bolmont et al., 2007; Hurtado et al., 2010; Lewis et al., 2001; Paulson et al., 2008; Perez et al., 2005; Seino et al., 2010; Terwel et al., 2008). The enhancement of tauopathy by Aß accumulation in APP/tau models has been described in some models as slow, developing with aging, and relatively modest (Paulson et al., 2008; Perez et al., 2005; Seino et al., 2010; Terwel et al., 2008). The mechanisms of worsened tau pathology in these APP/tau models are however not well understood, and potential additional misprocessing of tau in these APP/tau models compared to tau in FTD tau models has not been clarified. This link between Aß-mediated toxicity and tau pathology is relevant for the understanding of AD since tau pathology by itself can causes neurodegeneration (Ballatore et al., 2007).

The potential involvement of PS1 in modulation of tauopathy has also not been extensively investigated, except in the 3xTg-AD transgenic model in which expression of mutants APP, PS1 and P301L tau resulted in formation of amyloid deposits and accumulation of phosphorylated tau, although the potential enhancement of neurofibrillary degeneration compared to single P301L tau transgenic mice was not analyzed (Oddo et al., 2003).

To further investigate the misprocessing of tau and the modulation of tauopathy in experimental models developing an Aß pathology, we compared tau pathology and Aß load in a FTD mutant tau transgenic mice (Tg30), mutant APP/PS1 line transgenic mice (5xFAD) and in a new model resulting from their crossing. These APP/PS1xTg30 mice (named hereafter 5xFAD x Tg30) showed a severe enhancement of neurofibrillary degeneration associated to additional conformational, phosphorylation and cleavage changes in tau mimicking more closely than in Tg30 mice tau the modifications observed in PHF-tau in AD, and to an increased recruitment of endogenous wild-type mouse tau in NFT. These results suggest that mutant APP/PS1 or amyloid pathology was driving additional misprocessing of tau responsible for the acceleration and enhancement of tau pathology, a mechanism that might play a role in development of tau pathology and neuronal loss in AD.

2. Material and methods

Generation of 5xFAD x Tg30 mice

The transgenic mouse line Tg30 tau express a mutated tau transgene (1N4R human tau isoform bearing G272V and P301S mutations), under transcriptional control of the neuron-specific mouse thy-1 promoter (Schindowski et al., 2006) and has been described previously (Leroy et al., 2007). The Tg30 mice were maintained on C57Bl/6J genetic background and only heterozygous transgenic mice were used for this study. The 5xFAD double transgenic mice co-express and co-inherit the 695 amino acids isoform of the human amyloid precursor protein (APP695) carrying the Swedish, Florida, and London mutations and the human presenilin-1 (PS1) carrying the M146L and L286V mutations, both transgenes under the control of a thy-1 promoter (Tg6799 line) (Oakley et al., 2006). As for Tg30 mice, the 5xFAD mice were maintained on C57Bl/6J genetic background and only heterozygous transgenic mice were used for this study. The 5xFAD x Tg30 mice were obtained by crossing heterozygous transgenic 5xFAD mice with heterozygous transgenic Tg30 mice and maintained on C57Bl/6J genetic background. All transgenic animals were identified by polymerase chain reaction amplification of the human tau and human APP transgenes in genomic DNA as reported (Boutajangout et al., 2004; Leroy et al., 2012). Non-transgenic (named hereafter wild-type), Tg30, 5xFAD and 5xFAD x Tg30 mice from the same littermates were further analyzed. All studies on animals were performed in compliance and following approval of the ethical committee for the care and use of laboratory animals of the medical School of the Free University of Brussels.

Behavioural tests

To assess spatial memory and exploratory behaviour, spontaneous alternation and the number of arm entry were analyzed in 3-month-old mice using a Y-maze as described previously (Leroy et al., 2010). Briefly, mice were placed at the end of the first arm and left to explore the maze for 8 min. The mice movements were recorded with a camera and analyzed afterwards. The alternation percentage was calculated as the percentage of actual alternations to the possible number of arm entries. Global motor function and balance were assessed at 3, 6 and 8 months of age using the Rotarod test as described previously (Leroy et al., 2007). Briefly, mice were first submitted to training sessions (three trials per day during 3 consecutive days) during which they were placed on the rod rotating with a progressive acceleration from 4 to 40 rpm. Mice were evaluated using the same experimental setting throughout 300 seconds. The latency to fall off the Rotarod was

recorded. Animals staying more than 300 seconds were removed from the Rotarod and their latency fall recorded as 300 seconds.

Histological staining and immunohistochemistry

Mice were sacrificed by cervical dislocation and tissues were carefully dissected. Brain hemispheres and spinal cord were fixed in formalin solution (10%) during 24h followed by 2 hours of water wash before dehydratation in alcohol for paraffin embedding. Immunohistochemistry with diaminobenzidine as chromogen and the ABC method (Vector Laboratories) or double immunofluorescence with Alexa Fluor 488 and 594 species-specific conjugated secondary antibodies (Molecular Probes) was performed on 7 µm sagittal paraffin sections as described previously (Ando et al., 2011). For detection of amyloid plaques with anti-Aß antibodies, sections were first incubated 15 min in 100% (v/v) formic acid before peroxidase quenching. Tissue sections were examined with a Zeiss Axioplan I microscope (Carl Zeiss GmbH, Jena, Germany) and digital images acquired using an AxiocamHRc camera (Carl Zeiss). A panel of tau antibodies was used in this study to analyze tau pathology by immunohistochemistry and by immunoblotting (Ando et al., 2011; Brion et al., 1991a; Goedert et al., 1994; Goedert et al., 1995; Hanger et al., 2002; Hoffmann et al., 1997). Tau antibodies PHF1, CP13, Alz50, TG3 and MC1 were kindly provided by Dr. P. Davies (New York) (Jicha et al., 1997a; Jicha et al., 1997b; Otvos et al., 1994). The mTau-5 antibody to murine tau was a generous gift from M. Mercken, (Johnson&Johnson, Beerse, Belgium) (Sennvik et al., 2007). The 3H5 antibody to human APP was previously described (Philippe et al., 1996). The 2061 and 2104 antibodies to APP and APP phosphorylated on Thr668, respectively, were a generous gift of Dr. N. Sergeant (Inserm U837, Lille) (Sergeant et al., 2002).The SB129 antibody to PS1 was kindly provided by Dr. C. Van Broeckhoven (Antwerpen, Belgium)(Hendriks et al., 1998). The characteristics of all primary antibodies used in this study are summarized in Table 1.

The quantification of Aß plaque load or NFT was carried out on sagittal brain sections (from 0.75 to 1.5 mm of the midline, according to the Paxinos mouse brain atlas) and cross cervical spinal cord sections from 3-, 6-, and 9-month-old mice immunolabelled with anti-Aß40, anti-Aß42 antibodies or stained with the Gallyas silver-staining method. Virtual slices at 2,5X magnification (hippocampus and cortex) and 10X (spinal cord) were captured via a live video camera (CX9000, MBF Bioscience) mounted onto an optic microscope (AxioImager.M1, Zeiss) using StereoInvestigator program (version 8; MicroBrightField, Inc., Colchester, USA). During this acquisition, all parameters including lamp intensity, video camera setup, and calibration were maintained constant. Using ImageJ program (version 1.41o, NIH), the pictures were binarized to 8-

bit black and white images and the area covered by the extracellular Aß deposits in the cortex, hippocampus and spinal cord was measured with a fixed intensity threshold. Measurements of Aß positive areas were reported to the total area of the cerebral cortex, hippocampus or gray matter of spinal cord on each tissue section. As reported previously for Tg30 mice (Leroy et al., 2007), the number of Gallyas-positive cell profiles were counted in the cerebral cortex and the hippocampus, and their density (expressed as a number of cells/mm2) calculated after measurement of the surface of the cortex and the hippocampus on each tissue section using the ImageJ software (NIH). In the cervical spinal cord, Gallyas-positive cells were counted in the gray matter on 3 adjacent cross-sections per mice and their density reported to the surface of the gray matter in spinal cord sections.

Quantification of neuron number using design-based stereology

Stereological analysis was performed as described previously (Ando et al., 2011). Briefly, 15 µm thick coronal brain sections were stained with cresyl violet and the total number of hippocampal pyramidal cells in CA1, CA2, CA3 and CA4 sectors was estimated using 10-12 coronal sections at 225 µm intervals encompassing the whole hippocampus in one hemisphere of 9-month-old mice (wild-type, 5xFAD and 5xFAD x Tg30: n=6 and Tg30: n=5) by using a random-sampling stereological counting tool, the optical fractionator, with a stereology software (Stereoinvestigator version 8; MicroBrightField, Inc., Colchester, USA).

Immunoblot analysis

The brains and spinal cords from 3, 6, and 9-month-old mice were dissected and homogenized in either a 10-fold (brain) or a 20-fold (spinal cord) volume of modified RIPA buffer (50 mM Tris-HCl, pH 7.4, 1% Nonidet P-40, 0.25% (w/v) Na-deoxycholate, 150 mM NaCl, 1 mM PMSF (phenylmethylsulfonyl fluoride), leupeptin (25 µg/ml), pepstatin (25 µg/ml), 20 mM NaF, 1 mM sodium orthovanadate and 10 mM sodium pyrophosphate) as previously described (Ando et al., 2011). After centrifugation (20.000 x g for 20 minutes at 4°C), the supernatant was used for immunoblotting analysis. Samples (50 µg of protein/lane) were separated by 10% (w/v) or 12% (w/v) Glycine SDS-PAGE or 15% Tricine SDS-PAGE and transferred to nitrocellulose or PVDF membrane using a liquid transfer system (Bio-Rad). After blocking in skimmed milk the membranes were incubated with primary antibodies overnight followed by anti-rabbit or anti-mouse immunoglobulins (Sigma) conjugated to alkaline phosphatase for development with nitro blue tetrazolium and 5-bromo-4-chloro-3-indolyl phosphate or conjugated to horseradish peroxidase for development by chemiluminescence (Pierce* Fast Western Blot Kits, SuperSignal* West Pico, Thermo Scientific). The quantification of band intensity was performed by densitometry analysis

using the ImageJ program, and adjusted for protein loading based on immunoblots performed with the anti-β-actin, the anti-α-tubulin, and the B19 anti-tau antibodies.

Aβ40 and Aβ42 Electro-Chemiluminescence Immuno-Assay

Brains and spinal cord of 6-month-old mice were homogenized in RIPA buffer. After centrifugation, an aliquot of supernatant was kept to measure soluble Aβ whereas the pellet was resuspended in 3 volume of 100% formic acid to measure the insoluble Aβ. After an overnight incubation at 4°C under agitation, samples were centrifuged 30 min at 14000 rpm and 4°C, and then supernatants were neutralized in 20 volume of neutralization buffer (2M Tris-Base, 0.5M Na_2HPO_4, 0.05% NaN3). The protein concentration using the BioRad Protein Assay (BioRad) was measured also in the neutralized formic acid fraction to normalize the Aß levels to total brain or spinal cord protein concentration and to express the Aß load in nanograms per milligram of total protein. The concentration of Aβ40 and Aβ42 was measured by Electro-Chemiluminescence Immuno-Assay (ECLIA) as described previously (Leroy et al., 2012). Briefly, samples were analyzed using Meso Scale Discovery (MSD) SECTOR^{TM} Imager 2400 (Meso Scale Discovery, Gaithersburg, MD, USA), with the Aβ human triplex kit (MSD) according to the manufacturer's instructions.

Analysis of Sarkosyl-insoluble and soluble fractions

Sarkosyl-soluble and insoluble fractions were prepared from the brains and spinal cords from 6, 9 and 10-month-old mice as previously described (Ando et al., 2011). Briefly, after homogenization in RIPA buffer, homogenates were centrifuged and a same volume of supernatant was recovered for each sample, 1% (w/v) Sarkosyl was added and samples were incubated 30 min at room temperature under gently agitation. Samples were then ultracentrifugated during 30 min at 100 000g at 4°C. The supernatant corresponded to a Sarkosyl-soluble fraction, and the pellet, resuspended in 50 mM Tris (pH 7.4), corresponded to a Sarkosyl-insoluble fraction. Samples (50 µg of protein/lane for Sarkosyl-soluble fraction or 10 µl/lane for Sarkosyl-insoluble fraction) were separated on 10% (w/v) Glycine SDS-PAGE and further analyzed by immunoblotting.

Electron microscopy

Anesthetised mice were transcardially perfused with PBS followed by fixative (2% (w/v) paraformaldehyde and 2% (v/v) glutaraldehyde in 0.1 M phosphate buffer at pH 7.4). Tissue blocks of the hippocampus, of the cerebral cortex and of the spinal cord were quickly dissected and further fixed by immersion in 4% (w/v) glutaraldehyde in 0.1 M phosphate buffer at pH 7.4 for 90 min.

After washing in Millonig's buffer with 0.5% (w/v) sucrose for 24 h, the tissue blocks were postfixed in 2% (w/v) OsO4 for 30 min, dehydrated and embedded in Epon. Semi-thin sections were stained with toluidine blue. Ultrathin sections were counterstained with uranyl acetate and lead citrate and observed with a Zeiss EM 809.

Immunolabelling of tau filaments in electron microscopy

The pellet containing the Sarkosyl-insoluble material was resuspended in 50 mM Tris/HCl (pH 7.5). This material was adsorbed on formvar-carbon coated EM grids and immunolabelled and negatively stained with potassium phosphotungstate as reported (Brion et al., 1991b) with the BR21 rabbit anti-human tau antibody and the mTau5 mouse anti-murine tau followed by incubation with an anti-rabbit antibody conjugated to 15 nm gold particle and an anti-mouse antibody conjugated to 5 nm gold particle (Tebu Bio). Grids were viewed on a Zeiss EM 809 at 80 kV.

Statistical analysis

Statistical analysis was performed using Prism 4 (Graphpad Software). Kaplan-Meir survival curves were analyzed with Logrank tests. Statistical comparisons were performed using one or two-way ANOVA followed by a Bonferroni's Multiple Comparison Test or an unpaired t-test as noted in figure legends. Values of $P < 0.05$ were considered significant. Numbers of samples are indicated in the figure legends and histograms represent means ± SEM.

3. Results

Expression of mutant tau, APP and PS1 in 5xFAD x Tg30 mice

The expression of human tau, human APP and human PS1 transgenic proteins in the brain and spinal cord was analyzed by western blotting with human specific antibodies. Human tau proteins were expressed only in Tg30 and 5xFAD x Tg30 mice whereas human mutants PS1 and APP were expressed only in 5xFAD and in 5xFAD x Tg30 mice (Fig.1A). At 3 months (Fig. 1B) of age, the levels of human APP, human tau and human PS1 (full length or N-terminal fragment (NTF PS1)), were not significantly different in brain of 5xFAD x Tg30 mice compared to single 5xFAD mice, although tending to be lower in 5xFAD x Tg30 mice. The levels of human tau were also not significantly different in brain of 5xFAD x Tg30 mice compared to single Tg30 mice, and also tended to be lower in 5xFAD x Tg30 mice. At 9 months of age levels of human APP, human tau and human PS1 (full length or NTF PS1) were not significantly different, although human APP tended again to be lower in the 5xFAD x Tg30 mice (data not shown). In spinal cord, the level of human transgenes was not significantly different in 5xFAD x Tg30 transgenic mice compared to single transgenic mice at 3 months of age whereas at 9 months a significantly decreased level was observed for human APP and human PS1 (~ 42% and 30%, respectively) (data not shown). We observed by immunohistochemistry performed on brain and spinal cord tissue sections of 3-month-old mice (data not shown) that human proteins were expressed only in neurons in 5xFAD x Tg30 transgenic mice, as in the single 5xFAD and Tg30 mice. The neuroanatomical distribution of the APP and PS1 transgenic proteins in the nervous system was comparable in 5xFAD x Tg30 and 5xFAD mice, and the distribution of the tau transgenic protein was also similar in 5xFADx Tg30 and Tg30 mice.

5xFAD x Tg30 mice have a reduced survival and reduced body and brain weight as compared to Tg30 mice.

Analysis of Kaplan-Meir survival curves indicated that 5xFAD and 5xFAD x Tg30 mice exhibited a significantly decreased survival compared to wild-type mice at 10 months of age (Fig. 2). 5xFAD x Tg30 mice also showed a significantly decreased survival compared to Tg30 mice. Due to this reduced survival of 5xFAD x Tg30 mice after 10 months of age, we pooled data from mice of 9 and 10 months (referred to 9 months in the text) for all following quantitative measurements. 5xFAD x Tg30 mice also exhibited a significant and progressive reduction of their body weight from 6

months of age (data not shown) and a significant decrease of brain weight at 9 months of age compared to wild-type and 5xFAD mice (data not shown).

5xFAD x Tg30 mice have a more severe motor impairment than Tg30 mice

We next assessed motor function in the 4 different genotypes with the Rotarod test. Motor abilities were not different between mice of different genotypes at 3 months of age. A significant motor impairment was observed already in 6-month-old 5xFAD x Tg30 mice compared to all other genotypes (Fig. 3), whereas Tg30 mice displayed a significant motor impairment compared to wild-type and 5xFAD mice only at 8 months of age. At 6 and 8 months, motor impairment was higher in 5xFAD x Tg30 than in Tg30 mice. The analysis of spatial memory and of exploratory behaviour with the Y-maze test carried out at 3 months of age, before the appearance of motor deficits, did not show any significant differences between genotypes (wild-type, n=19; 5xFAD, n=19; Tg30, n=18; 5xFAD x Tg30, n=11) (data not shown). Thus, 5xFAD x Tg30 mice did not show alterations of spatial memory in Y-maze test at 3 months but exhibited a more severe motor impairment than Tg30 mice at older age.

Loss of pyramidal neurons in hippocampus of 5xFAD x Tg30 mice

Neuronal loss has not been systematically assessed in bigenic APP/tau models and we assessed the extent of neuronal loss by performing a stereological cell count of the total number of neurons in pyramidal layers (CA1 to CA4) of hippocampus of 9-month-old mice in the 4 different genotypes. The numbers of pyramidal neurons were not significantly different between wild-type (441892 ± 28990, n=6), 5xFAD (474366 ± 18776, n=6) and Tg30 (473421 ± 37772, n=5) mice. The number of pyramidal neurons was however significantly decreased in 5xFAD x Tg30 mice (355467 ± 22643, n=6, mean+/- SEM), compared to 5xFAD and Tg30 mice ($p< 0.05$, by one-way Anova followed by a Bonferroni's Multiple Comparison Test) (data not shown).

5xFAD x Tg30 mice develop both NFT and neuritic plaques with PHF-containing dystrophic neurites

5xFAD x Tg30 mice developed both NFT and amyloid plaques as shown by double immunolabelling with tau and Aβ antibodies (Fig. 4A). NFT in hippocampal neurons (Fig. 4B were composed of straight filaments with a wavy appearance and of occasional PHF (Fig. 4C), as described previously in Tg30 mice (Leroy et al., 2007). To determine the contribution of tau pathology to neuritic plaques, we analyzed the neuritic components of neuritic plaques in 9-month-

old 5xFAD and 5xFAD x Tg30 mice. Only 5xFAD x Tg30 mice exhibited dilated dystrophic neurites positive for human tau and Gallyas positive neurites (data no shown). Ultrastructural observations of neuritic plaques showed that some plaque-associated dystrophic neurites contained PHF in 5xFAD x Tg30 mice (Fig. 4D and E) and never in 5xFAD mice.

Increased density of Gallyas positive NFT in brain of 5xFAD x Tg30 compared to Tg30 mice

As reported before, Tg30 mice showed an age-dependent increase from 3 to 9 months of age of Gallyas-positive NFT in hippocampus, cerebral cortex and spinal cord, with early appearance of NFT in the spinal cord (Leroy et al., 2007). The 5xFAD x Tg30 mice showed a similar age-dependent increase of NFT. The density of Gallyas-positive cells in hippocampus (Fig. 5A, D) and in cerebral cortex (Fig 5B, E) was however systematically higher in 5xFAD x Tg30 mice compared to Tg30 mice and dramatically increased at 9 months of age in 5xFAD x Tg30 mice. In the spinal cord, the density of NFT increased strongly (~10-fold) from 3 to 9 months of age in both genotypes and was systematically slightly higher in 5xFAD x Tg30 mice but was not significantly different between the two genotypes (Fig. 5C, F).

Increased and accelerated generation of insoluble tau in 5xFAD x Tg30 mice compared to Tg30 mice

Since the density of Gallyas-positive cells in the brain was higher in 5xFAD x Tg30 mice than in Tg30 mice, we investigated the levels of insoluble tau in both genotypes at 6 and 9 months of age. Sarkosyl-insoluble tau was not present in wild-type and 5xFAD mice but a major 62-64 kDa tau species was identified in Tg30 and 5xFAD x Tg30 mice (Fig. 6A). In the brain, the level of insoluble tau proteins increased progressively with age in both Tg30 and 5xFAD x Tg30 mice. Compared to Tg30 mice, the level of total (human and mouse) insoluble tau and of insoluble human tau in 5xFAD x Tg30 mice were 2- and 2.4-fold higher, respectively, at 6 months of age (not shown), and were 3.6- and 3-fold higher, respectively, at 9 months of age (Fig. 6B). In the spinal cord of 5xFAD x Tg30 mice, a slightly higher level of insoluble tau was observed at 9 months of age (x 1.5-fold for total tau and x 1.7-fold for insoluble human tau) (data not shown). Thus, compared to Tg30 mice, the generation of abnormal Sarkosyl-insoluble tau in 5xFAD x Tg30 mice was not only increased, but was also accelerated with age and this age-associated acceleration was more marked in the brain than in the spinal cord.

Increased abnormal phosphorylation, conformation and caspase cleavage of insoluble tau in 5xFAD x Tg30 mice compared to Tg30 mice

We next compared Sarkosyl-insoluble tau in brain of 9-month-old 5xFAD x Tg30 and Tg30 mice using several antibodies recognizing conformation and post-translational modifications characteristic of PHF-tau in AD. The MC1 antibody that recognizes a pathological conformation of tau (Jicha et al., 1997a; Weaver et al., 2000) labelled insoluble tau in 5xFAD x Tg30 and in Tg30 mice but the level of insoluble MC1 positive tau (normalized to total tau) was higher in 5xFAD x Tg30 mice than in Tg30 mice (Fig. 6C and D). Insoluble tau was also more immunoreactive in 5xFAD x Tg30 than in Tg30 mice with the AT100 antibody (pThr212/217 and pSer214) (Hoffmann et al., 1997) (Fig 6C and E). Insoluble tau was immunoreactive 5xFAD x Tg30 mice and not in Tg30 mice with the TG-3 antibody detecting a conformation and abnormal phospho-tau epitope (pThr231) in PHF (Jicha et al., 1997b) and with the Alz50 antibody, detecting an early stage abnormal conformation of tau (Jicha et al., 1997a) (Fig 6C). Insoluble caspase-cleaved tau (detected with the tau Asp421 antibody) was detected in brain of 5xFAD x Tg30 mice but not in Tg30 mice (Fig. 6C). Thus, insoluble tau in the brain of 5xFAD x Tg30 mice exhibited more severe conformational, abnormal phosphorylation and caspase-cleavage changes than in Tg30 mice.

Increased hyperphosphorylation of insoluble and soluble tau in 5xFAD x Tg30 mice compared to Tg30 mice

We then compared the hyperphosphorylation state of insoluble and soluble tau in brain of 9-month-old Tg30 and 5xFAD x Tg30 mice, using several phosphotau antibodies that recognizes phosphotau epitopes found in normal tau. The degree of phosphorylation of insoluble phospho-tau in brain (normalized to total tau) was significantly higher in 5xFAD x Tg30 mice at 9 months for pSer202 tau (CP13), pSer202/205 tau (AT8) and pThr231/Thr235 tau (AT180) compared to Tg30 mice (Fig. 7A, C) and was similar in spinal cord of both transgenic mice (data not shown). Insoluble phosphorylated tau species with a higher electrophoretic mobility (arrows in Fig. 7A) were detected only in 5xFAD x Tg30 mice and could correspond to cleaved tau fragments (fig. 7A). The degree of phosphorylation of soluble phospho-tau (normalized to total tau) was significantly higher for pThr181 (AT270), pSer202 tau (CP13) and pSer396/404 (PHF-1) in brain of 5xFAD x Tg30 mice compared to Tg30 mice (Fig. 7B, D) and was not significantly different in spinal cord of both transgenic mice (data not shown). Soluble phosphorylated tau species with a slower electrophoretic mobility (arrows in Fig. 7B) were also much more abundant in brain of 5xFAD x Tg30 mice than in Tg30 mice. Thus the degree of phosphorylation of insoluble and soluble tau proteins was much higher in brain of 5xFAD x Tg30 than in Tg30 mice.

Recruitment of murine tau into PHF in 5xFAD x Tg30 mice

We next compared the recruitment of endogenous murine tau into insoluble tau and into PHF in 5xFAD x Tg30 mice and in Tg30 mice. The anti-murine tau antibody mTau5 detected high levels of insoluble murine tau in brain of 10-month-old 5xFAD x Tg30 mice but not in Tg30 mice (Fig. 8A). Insoluble murine tau was detected in spinal cord of both transgenic lines (data not shown). The BR10 antibody (specific for 2N tau isoforms) labelled insoluble tau species corresponding to murine tau and not human tau since the human transgenic tau is a 1N4R tau isoform (data not shown). Isolated PHF present in insoluble brain fractions were then analyzed by immunolabelling in electron microscopy for their content in murine tau. Isolated PHF were systematically labelled by the human tau antibody BR21 (Fig. 8B) in Tg30 and 5xFAD x Tg30 mice. Murine tau identified by mTau5 antibody was however very weakly detected in isolated PHF of Tg30 mice but was abundant in isolated PHF of 5xFAD x Tg30 mice (Fig. 8B). In 5xFAD x Tg30 mice, some PHF were also clearly composed of both human and mouse tau as shown by double immunolabelling (Fig. 8B). Thus, murine tau was more abundant in insoluble fraction and also more frequently integrated into PHF from brain of 5xFAD x Tg30 compared to Tg30 mice.

Reduced amyloid pathology in brain and in spinal cord of 5xFAD x Tg30 mice

To compare the age-dependent development of amyloid pathology in 5xFAD and 5xFAD x Tg30 mice, brain and spinal cord sections of 3-, 6- and 9-month-old transgenic mice were labelled with anti-Aβ40 and anti-Aβ42 antibodies. Aβ40 and Aβ42 positive plaques were first found at 3 months in subiculum and frontal cortex in young mice and they spread out later in the whole cerebral cortex, the hippocampus, subcortical nuclei, the brainstem and the spinal cord of both genotypes (Fig. 9A). The quantification of the Aß40 and Aß42 amyloid plaque load in hippocampus, cerebral cortex and gray matter of the spinal cord confirmed their increase in an age-dependent manner in both 5xFAD and 5xFAD x Tg30 mice (Fig. 9B, C, D). However, the Aß40 and Aß42 amyloid plaque load was lower (except at 6 months in hippocampus and cortex for Aß42) in 5xFAD x Tg30 mice than in 5xFAD mice at each age, and was highly significantly decreased in the spinal cord. By western-blotting analysis, we measured a significant lower Aβ level in brain (Fig 10A and C) and in spinal cord (Fig 10B and D) in 9-month-old 5xFAD x Tg30 mice compared to 5xFAD mice. Measurements of soluble and insoluble Aβ42 (data not shown) and Aβ40 (supplementary Fig. 1) by Electro-Chemiluminescence Immuno-Assay also showed their systematic lower levels in brain and spinal cord of 5xFAD x Tg30 mice. A decrease of β-CTFs levels in spinal cord and in brain were

also observed in 5xFAD x Tg30 mice (Fig. 10C and D). Since APP phosphorylation modulates its amyloidogenic processing, we analyzed APP phosphorylation using the antibody to APP phosphorylated at Thr668. In the brains of 5xFAD xTg30 mice, the levels of phosphorylated CTFs were significantly reduced and levels of phosphorylated APP holoprotein also showed a trend towards reduction (supplementary Fig 2). Thus amyloid pathology developed and progressively spread out in brain and spinal cord of both 5xFAD and 5xFAD x Tg30 mice but was reduced in 5xFAD x Tg30 mice.

4. Discussion

To analyze and adequately compare misprocessing of tau and generation of NFT in a mutant tau mouse without and with concomitant development of Aß pathology, we crossed 5xFAD mice, an AD amyloid model co-expressing mutants human APP and PS1 with Tg30 mice, a mouse model of tauopathy overexpressing mutant human tau. Crossing of 5xFAD mice with Tg30 mice allowed adequate comparison of behavioral deficits, NFT, tau misprocessing and Aß levels between 5xFAD, Tg30 and 5xFAD x Tg30 mice, an analysis that cannot be easily achieved in homozygote models co-expressing these three transgenes and breeding as single-transgenic lines such as the 3xTg-AD transgenic model (Oddo et al., 2003). Comparisons of behavioural and pathological features of the different lines are summarized in Table 2.

Severe enhancement of neurofibrillary pathology in 5xFAD x Tg30 mice compared to Tg30 mice

Tau pathology was dramatically more severe in brain of 5xFAD x Tg30 mice than in Tg30 mice, as shown by severely increased density of NFT and levels of insoluble tau. These observations are in agreement with previous studies in which various degrees of enhancement of NFT pathology were observed in transgenic mouse models combining expression of human mutant tau and APP (Bolmont et al., 2007; Hurtado et al., 2010; Lewis et al., 2001; Paulson et al., 2008; Perez et al., 2005; Seino et al., 2010; Terwel et al., 2008). An additional acceleration of the spatiotemporal progression of tau pathology was however observed in the present 5xFAD x Tg30 model, since the density of NFT was not only systematically higher in 5xFAD x Tg30 mice at all ages, but NFT density increased with age more severely in 5xFAD x Tg30 than in Tg30 mice. This much severe increase of tau pathology in 5xFAD x Tg30 mice was not due to increased expression of tau since levels of human tau and of total tau proteins were not different between 5xFAD x Tg30 and Tg30 mice. Compared to previous models expressing only mutant APP and mutant tau, the severe increase of NFT pathology observed in 5xFAD x Tg30 mice might be related to the additional expression of mutant PS1. In 5xFAD mice, combined expression of mutants APP and PS1 is additive and enhances generation of total Aß and of Aß42 compared to mice expressing only the APPsw mutation (Oakley et al., 2006). Thus relatively higher production of Aß and Aß42 in 5xFAD mice could be responsible for the much enhanced tau pathology in 5xFAD x Tg30 mice. However, mutant PS1 (Tanemura et al., 2006) also enhances tau phosphorylation through Aß-

independent pathways, that might play a role in the observed enhancement of tau pathology in 5xFAD x Tg30 mice.

Increased phosphorylation, misfolding and truncation of tau in 5xFAD x Tg30 mice

Insoluble tau in 5xFAD x Tg30 mice, compared to Tg30 mice, exhibited unpreviously described additional post-translational changes mimicking more closely the post-translational changes characteristic of PHF-tau in AD. Indeed we observed that insoluble tau in 5xFAD x Tg30 mice was more highly phosphorylated than in Tg30 on several phosphotau epitopes. Insoluble tau in 5xFAD x Tg30 mice also showed abnormal conformational epitopes typical of PHF-tau in AD and either absent or fainter in tau in Tg30 mice. In addition, we found a significantly higher degree of phosphorylation of soluble tau in 5xFAD x Tg30 mice compared toTg30 mice. We also observed higher proteolytic changes of tau in 5xFAD x Tg30 than in Tg30 mice. First, we observed that the antibody to Asp421 cleaved tau, a cleavage generated by caspase-3 (Gamblin et al., 2003; Rissman et al., 2004), labelled insoluble tau in 5xFAD x Tg30 mice, but not in Tg30 mice, as observed previously in the latter mice (Leroy et al., 2007). Caspase cleavage of tau accelerates nucleation-dependent assembly of tau into filaments (Gamblin et al., 2003; Rissman et al., 2004). Caspase cleaved tau is also preferentially recognized by the conformation-dependent MC1 tau antibody (Rissman et al., 2004), and insoluble tau was more strongly MC1 positive in 5xFAD x Tg30 mice than in Tg30 mice. Aß treatment of neurons induces caspase-3 cleavage of tau (Gamblin et al., 2003) (Rissman et al., 2004), and thus Aß generated in 5xFAD x Tg30 mice, and not in Tg30 mice, might be responsible for caspase activation and tau cleavage in 5xFAD x Tg30 mice. 5xFAD x Tg30 mice also showed increased levels of cleaved tau fragments with lower molecular weights. Tau fragments containing the repeat domain are efficient for nucleation of tau into PHF (Wang et al., 2007) and these cleaved fragments display a high tendency for aggregation. Altogether, this suggests that increased tau phosphorylation, enhanced conformational changes and truncation events were promoting and accelerating tau aggregation in 5xFAD x Tg30 mice compared to Tg30 mice.

Higher recruitment of murine tau into PHF in 5xFAD x Tg30 mice

In addition to increased levels of insoluble human tau, we also detected high levels of insoluble endogenous murine tau in brains of 9-month-old 5xFAD x Tg30 mice, but not in Tg30 mice and high co-integration of murine tau with human tau in brain NFT and in isolated PHF of 5xFAD x Tg30 mice. A low level of recruitment of murine tau into PHF has been reported previously in 12-month-old Tg30 mice (Ando et al., 2011) and in other mutant tau mice (Allen et

al., 2002). Murine tau might not have the same propensity for aggregation as human tau *in vivo*: e.g. tau pathology in Tg30 mutant tau mouse is exacerbated by tau depletion of mouse tau (Ando et al., 2011), and propagation of tau aggregation by stereotaxic injection of PHF-tau proteins was efficient in mice expressing human tau but not in wild-type mice expressing endogenous murine tau (Clavaguera et al., 2009). Nevertheless, overexpresion of human mutant tau restricted to the entorhinal cortex led to propagation of tau pathology with recruitment of endogenous mouse tau in another model (de Calignon et al., 2012), indicating that mouse tau has the ability to aggregate. Amyloid pathology in APP or APP/PS1 transgenic models is not able per se to induce recruitment of endogenous murine tau into NFT, even in presence of wild-type human tau (Boutajangout et al., 2004). Thus even in presence of Aß, some "seeding" by expression of a mutant human tau as in the present 5xFAD x Tg30 mice seems needed to generate an efficient integration of mouse tau into PHF, an integration that can then propagate by itself (Van der Jeugd et al., 2012). This high recruitment of murine tau was not reported in previous bigenic APP/tau mice. Interestingly, murine tau did co-aggregate efficiently with truncated human mutant tau in an inducible mouse model (Mocanu et al., 2008). The increased levels of cleaved tau fragments that we observed in 5xFAD x Tg30 mice might thus plays a role in the higher recruitment of murine tau in PHF in the latter mice compared to Tg30 mice.

Reduced amyloid pathology in 5xFAD x Tg30 mice compared to 5xFAD mice

The amyloid pathology increased in an age-dependent manner in both 5xFAD and 5xFAD x Tg30 mice, but was lower in 5xFAD x Tg30 mice than in 5xFAD mice. This decrease was observed for both extracellular and insoluble and soluble Aß40 and Aß42. Interestingly, we observed that levels of ß-CTFs and of phosphorylated ß-CTFs were lower in brain of 5xFAD x Tg30 than in 5xFAD mice. APP phosphorylation at Thr668 has been reported to facilitate BACE1 cleavage (Lee et al., 2003) and intraneuronal accumulation of Aß (Pierrot et al., 2006), and ß-CTFs phosphorylation was found to facilitate γ-secretase cleavage (Vingtdeux et al., 2005). These observations suggest that ß-amyloidogenic processing of APP was lower in 5xFAD x Tg30 than in 5xFAD mice. The trend for reduced expression of human mutant APP protein in brain and the significantly reduced expression of human APP and human PS1 in spinal cord could be responsible for the decreased amyloid pathology observed in 9-month-old 5xFAD x Tg30 mice compared to 5xFAD mice. Other mechanisms such as interference with APP trafficking due to tau pathology are however not excluded. Also, tau deletion can reduce amyloidogenic processing of APP (Leroy et al., 2012) and increased tau pathology in 5xFAD x Tg30 mice with segregation of tau in NFT could have the same effect. The high reduction of Aß load in the spinal cord of 5xFAD x Tg30 mice

could explain that tau pathology was less markedly enhanced in the spinal cord than in the brain of these mice.

Despite this reduction of Aß load, aged 5xFAD x Tg30 mice showed a significant neuronal loss in the hippocampus compared to 5xFAD and to Tg30 mice. This suggests that the neuronal loss in 5xFAD x Tg30 mice was more closely related to their more severe tau pathology, and to the presence of abnormal tau proteins mimicking more closely the abnormal tau proteins found in AD. When compared to their littermates 5xFAD and Tg30 mice, 5xFAD x Tg30 mice showed a reduced survival. This increased mortality in 5xFAD x Tg30 mice was most probably related to their more severe motor deficits that were higher than in Tg30 and 5xFAD mice at all ages. Compared to Tg30 and 5xFAD mice, the combined tau and amyloid pathology in the spinal cord of 5xFAD x Tg30 mice might accelerate their motor deficits.

In conclusion, we show here by analyzing three different transgenic genotypes that co-expression of mutants APP and PS1 in a tau mutant mice dramatically increased in their brain the formation of NFT, the yield of phosphorylated soluble and insoluble tau, the recruitment of endogenous wild-type tau and neuronal loss. Insoluble tau in 5xFAD x Tg30 mice showed additional conformational, phosphorylation, and truncation changes compared to insoluble tau in Tg30 mice, mimicking more closely the post-translational changes of PHF-tau in AD. This 5xFAD x Tg30 model might thus be a better model to study the misprocessing of tau in presence of an amyloid pathology, as observed in AD.

Acknowledgements: This study was supported by grants from the Diane program (Walloon region) (816856) and from the Fonds de la Recherche Scientifique Médicale (3.4504.10) and performed in the frameship of the Interuniversity Attraction Poles program (P7/16) of the Belgian Federal Science Policy Office. We thank Dr R. Vassar (Northwestern University, Chicago) for providing the Tg6799 APP/PS1 mice and Dr Luc Buée (INSERM, U837, Lille) for providing the Tg30 line.

References

Allen, B., et al., 2002. Abundant tau filaments and nonapoptotic neurodegeneration in transgenic mice expressing human P301S tau protein. J Neurosci. 22, 9340-51.

Ando, K., et al., 2011. Accelerated human mutant tau aggregation by knocking out murine tau in a transgenic mouse model. Am J Pathol. 178, 803-16.

Ballatore, C., et al., 2007. Tau-mediated neurodegeneration in Alzheimer's disease and related disorders. Nature Reviews Neuroscience. 8, 663-672.

Bolmont, T., et al., 2007. Induction of tau pathology by intracerebral infusion of amyloid-beta - containing brain extract and by amyloid-beta deposition in APP x Tau transgenic mice. Am J Pathol. 171, 2012-20.

Boutajangout, A., et al., 2004. Characterisation of cytoskeletal abnormalities in mice transgenic for wild-type human tau and familial Alzheimer's disease mutants of APP and presenilin-1. Neurobiol Dis. 15, 47-60.

Brion, J. P., et al., 1991a. Tau in Alzheimer neurofibrillary tangles. N- and C-terminal regions are differentially associated with paired helical filaments and the location of a putative abnormal phosphorylation site. Biochem J. 273(Pt 1), 127-33.

Brion, J. P., et al., 1991b. A68 proteins in Alzheimer's disease are composed of several tau isoforms in a phosphorylated state which affects their electrophoretic mobilities. Biochem J. 279 (Pt 3), 831-6.

Brion, J. P., et al., 1985. Mise en évidence immunologique de la protéine tau au niveau des lésions de dégénérescence neurofibrillaire de la maladie d'Alzheimer. Arch.Biol.(Brux). 95, 229-235.

Buée, L., et al., 2000. Tau protein isoforms, phosphorylation and role in neurodegenerative disorders. Brain Res.Rev. 33, 95-130.

Clavaguera, F., et al., 2009. Transmission and spreading of tauopathy in transgenic mouse brain. Nat Cell Biol. 11, 909-13.

de Calignon, A., et al., 2012. Propagation of tau pathology in a model of early Alzheimer's disease. Neuron. 73, 685-97.

Gamblin, T. C., et al., 2003. Caspase cleavage of tau: linking amyloid and neurofibrillary tangles in Alzheimer's disease. Proc Natl Acad Sci U S A. 100, 10032-7.

Goedert, M., et al., 1994. Epitope mapping of monoclonal antibodies to the paired helical filaments of Alzheimer's disease: Identification of phosphorylation sites in tau protein. Biochem.J. 301, 871-877.

Goedert, M., et al., 1995. Monoclonal antibody AT8 recognises tau protein phosphorylated at both serine 202 and threonine 205. Neurosci.Lett. 189, 167-170.

Gotz, J., et al., 2001. Formation of neurofibrillary tangles in P301l tau transgenic mice induced by Abeta 42 fibrils. Science. 293, 1491-5.

Grundke-Iqbal, I., et al., 1986. Abnormal phosphorylation of the microtubule-associated protein tau (tau) in Alzheimer cytoskeletal pathology. Proc Natl Acad Sci U S A. 83, 4913-7.

Hanger, D. P., et al., 2002. The complex relationship between soluble and insoluble tau in tauopathies revealed by efficient dephosphorylation and specific antibodies. FEBS Lett. 531, 538-42.

Hardy, J., Selkoe, D. J., 2002. Medicine - The amyloid hypothesis of Alzheimer's disease: Progress and problems on the road to therapeutics. Science. 297, 353-356.

Hendriks, L., et al., 1998. Immunoreactivity of presenilin-1 and tau in Alzheimer's disease brain. Exp Neurol. 149, 341-8.

Hoffmann, R., et al., 1997. Unique Alzheimer's disease paired helical filament specific epitopes involve double phosphorylation at specific sites. Biochem. 36, 8114-8124.

Hurtado, D. E., et al., 2010. A{beta} accelerates the spatiotemporal progression of tau pathology and augments tau amyloidosis in an Alzheimer mouse model. Am J Pathol. 177, 1977-88.
Jicha, G. A., et al., 1997a. Alz-50 and MC-1, a new monoclonal antibody raised to paired helical filaments, recognize conformational epitopes on recombinant tau. J Neurosci Res. 48, 128-32.
Jicha, G. A., et al., 1997b. A conformation- and phosphorylation-dependent antibody recognizing the paired helical filaments of Alzheimer's disease. J Neurochem. 69, 2087-95.
Lee, M. S., et al., 2003. APP processing is regulated by cytoplasmic phosphorylation. J Cell Biol. 163, 83-95.
Leroy, K., et al., 2010. Lithium treatment arrests the development of neurofibrillary tangles in mutant tau transgenic mice with advanced neurofibrillary pathology. J Alzheimers Dis. 19, 705-19.
Leroy, K., et al., 2012. Lack of Tau Proteins Rescues Neuronal Cell Death and Decreases Amyloidogenic Processing of APP in APP/PS1 Mice. Am J Pathol. 181, 1928-40.
Leroy, K., et al., 2007. Early axonopathy preceding neurofibrillary tangles in mutant tau transgenic mice. Am J Pathol. 171, 976-92.
Lewis, J., et al., 2001. Enhanced neurofibrillary degeneration in transgenic mice expressing mutant tau and APP. Science. 293, 1487-1491.
Mocanu, M. M., et al., 2008. The potential for beta-structure in the repeat domain of Tau protein determines aggregation, synaptic decay, neuronal loss, and coassembly with endogenous Tau in inducible mouse models of tauopathy. Journal of Neuroscience. 28, 737-748.
Oakley, H., et al., 2006. Intraneuronal beta-amyloid aggregates, neurodegeneration, and neuron loss in transgenic mice with five familial Alzheimer's disease mutations: potential factors in amyloid plaque formation. J Neurosci. 26, 10129-40.
Oddo, S., et al., 2003. Triple-transgenic model of Alzheimer's disease with plaques and tangles: intracellular Abeta and synaptic dysfunction. Neuron. 39, 409-21.
Otvos, L., Jr., et al., 1994. Monoclonal antibody PHF-1 recognizes tau protein phosphorylated at serine residues 396 and 404. J.Neurosci.Res. 39, 669-673.
Paulson, J. B., et al., 2008. Amyloid plaque and neurofibrillary tangle pathology in a regulatable mouse model of Alzheimer's disease. Am J Pathol. 173, 762-72.
Perez, M., et al., 2005. Characterization of a double (amyloid precursor protein-tau) transgenic: tau phosphorylation and aggregation. Neuroscience. 130, 339-47.
Philippe, B., et al., 1996. Generation of a monoclonal antibody to the carboxy-terminal domain of tau by immunization with the amino-terminal domain of the amyloid precursor protein. J Neurosci Res. 46, 709-19.
Pierrot, N., et al., 2006. Calcium-mediated transient phosphorylation of tau and amyloid precursor protein followed by intraneuronal amyloid-beta accumulation. J Biol Chem. 281, 39907-14.
Rissman, R. A., et al., 2004. Caspase-cleavage of tau is an early event in Alzheimer disease tangle pathology. J Clin Invest. 114, 121-30.
Schindowski, K., et al., 2006. Alzheimer's disease-like tau neuropathology leads to memory deficits and loss of functional synapses in a novel mutated tau transgenic mouse without any motor deficits. Am J Pathol. 169, 599-616.
Seino, Y., et al., 2010. Amyloid beta accelerates phosphorylation of tau and neurofibrillary tangle formation in an amyloid precursor protein and tau double-transgenic mouse model. J Neurosci Res. 88, 3547-54.
Sennvik, K., et al., 2007. Tau-4R suppresses proliferation and promotes neuronal differentiation in the hippocampus of tau knockin/knockout mice. Faseb Journal. 21, 2149-2161.
Sergeant, N., et al., 2002. Progressive decrease of amyloid precursor protein carboxy terminal fragments (APP-CTFs), associated with tau pathology stages, in Alzheimer's disease. J Neurochem. 81, 663-72.

Tanemura, K., et al., 2006. Formation of tau inclusions in knock-in mice with familial Alzheimer disease (FAD) mutation of presenilin 1 (PS1). J Biol Chem. 281, 5037-41.
Terwel, D., et al., 2008. Amyloid activates GSK-3 beta to aggravate neuronal tauopathy in bigenic mice. American Journal of Pathology. 172, 786-798.
Van der Jeugd, A., et al., 2012. Cognitive defects are reversible in inducible mice expressing pro-aggregant full-length human Tau. Acta Neuropathol. 123, 787-805.
Vingtdeux, V., et al., 2005. Phosphorylation of amyloid precursor carboxy-terminal fragments enhances their processing by a gamma-secretase-dependent mechanism. Neurobiology of Disease. 20, 625-637.
Wang, Y. P., et al., 2007. Stepwise proteolysis liberates tau fragments that nucleate the Alzheimer-like aggregation of full-length tau in a neuronal cell model. Proc Natl Acad Sci U S A. 104, 10252-7.
Weaver, C. L., et al., 2000. Conformational change as one of the earliest alterations of tau in Alzheimer's disease. Neurobiol Aging. 21, 719-27.

Legends of Figures

Figure 1

Levels of APP, PS1 and tau proteins are similar in 5xFAD x Tg30 compared to Tg30 or 5xFAD mice

Western blotting and densitometry analysis on brain homogenates.

A) Representative Western blots with the B19 anti-tau antibody (murine and human tau), the BR21 human specific tau antibody (human tau), the SB129 anti-PS1 antibody (murine and human full-length and N-terminal fragment of PS1), the MAB1563 human specific PS1 antibody, the 2061 antibody to APP (murine and human APP), the 3H5 human specific APP antibody, and the anti-actin antibody, in wild-type, 5xFAD, Tg30 and 5xFAD x Tg30 mice. 5xFAD xTg30 mice express the human mutant tau, PS1 and APP proteins. Human PS1 N-terminal fragment (PS1 NTF) is present only in 5xFAD and 5xFAD x Tg30 mice.

B) Densitometry quantification. There is a similar level of total tau proteins in Tg30 and 5xFAD x Tg30 mice and of total APP and PS1 in 5xFAD and 5xFAD x Tg30 mice. Each human transgenic protein was also expressed at a similar level in 5xFAD x Tg30 mice and in corresponding single transgenic mice. All data were normalized to their respective actin expression level. The statistical difference was evaluated by a one-way Anova followed by a Bonferroni's Multiple Comparison Test for total tau, APP and PS1 (at least 7 mice per genotype) (*, $p<0.05$ and ***, $p<0.0001$: significantly different from wild-type mice; ###, $p<0.0001$: significantly different from 5xFAD mice; &&&, $p<0.0001$: significantly different from Tg30 mice) and by an unpaired t-test for human transgenes.

Figure 2

Decreased survival in 5xFAD x Tg30 mice.

Kaplan-Meier survival curves. Decreased survival of 5xFAD x Tg30 mice compared to wild-type and Tg30 mice and of 5xFAD mice compared to wild-type mice. Transgenic and wild-type mice were followed up to 10 months after birth (wild-type, n=25; 5xFAD, n=18; Tg30, n=22; 5xFAD x Tg30, n=28). The statistical difference was evaluated by a Logrank test (*, $p<0.05$ and **, $p<0.01$: significantly different from wild-type mice; &, $p<0.05$: significantly different from Tg30 mice.)

Figure 3

More severe motor deficits in 5xFAD x Tg30 mice.

Rotarod testing. Compared to all other genotypes, the 5xFAD x Tg30 mice displayed a significant motor deficit at 6 months of age whereas Tg30 mice showed a significant motor deficit only at 8 months of age. The statistical difference was evaluated by a two-way Anova followed by a Bonferroni's Multiple Comparison Test (wild-type, n=39, 44, 30; 5xFAD, n=28, 35, 26; Tg30, n=40, 35, 28; 5xFAD x Tg30, n=28, 29, 20 at 3, 6 and 8 months of age, respectively). §§§, $p<0.0001$: significantly different from wild-type mice at the same age; #, $p<0.05$ and ###, $p<0.0001$: significantly different from 5xFAD mice at the same age; &&&, $p<0.0001$: significantly different from Tg30 mice at the same age.

Figure 4

Neuritic plaques and NFT in 5xFAD xTg30 mice.

Representative illustrations of NFT and neuritic plaques co-existence in the brain of a 9 month-old 5xFAD x Tg30 mouse,

A) Light microscopy. Double immunofluorescent labelling in the cortex with the anti-phosphotau PHF-1 (red) and the anti-Aß42 (green) antibodies. NFT and amyloid plaques are numerous in cortical layers.

B- E) Transmission electron microscopy. Ultrathin sections.

B) Cerebral cortex. An amyloid deposit (A) is surrounded by dystrophic neurites containing accumulations of vesicular structures.

C) Magnification of the area delimited (black rectangle) in (B). This degenerating neurite contains wavy filaments.

D) Hippocampus (Ammon's horn). A neuron contains a fibrillar inclusion (NFT) filling most of its pericaryon.

E) Magnification of the area delimited (black rectangle) in (D). The NFT is composed of bundles of wavy filaments and of paired helical filaments (arrows).

Scale bars: A: 100 µm; B: 1 µm; C: 50 nm; D: 1 µm; E: 200 nm.

Figure 5

Severe increase of NFT density in brain of 5xFAD x Tg30 mice compared to Tg30 mice.

A - C) Gallyas silver staining on tissue sections from hippocampus (A), cerebral cortex (B) and spinal cord (C) of 9-month-old Tg30 (left panels) and 5xFAD x Tg30 mice (right panels). A much

higher density of NFT is observed in the hippocampus and the cerebral cortex of 5xFAD xTg30 mice, but not in the spinal cord. CA1: layer 1 of pyramidal cells in the Ammon's Horn.

D - F) Quantification of the density of Gallyas-positive neuronal inclusions in Tg30 and 5xFAD x Tg30 mice. NFT were already detected at 3 months of age and showed an age-dependent increase in their density in both genotypes. NFT density was much higher at 9 months in hippocampus (D) and cerebral cortex (E) of 5xFAD x Tg30 mice compared to Tg30 mice. At 6 months, NFT density was highest in the spinal cord (F) but similar in both genotypes. The statistical difference was evaluated by a two-way Anova followed by post hoc comparisons using Bonferroni's Multiple Comparison Test (hippocampus and cerebral cortex: Tg30, n=9 at 3 and 6 and n=13 at 9 months of age, 5xFAD x Tg30, n=7, 5 and 10 at 3, 6 and 9 months of age, respectively; Spinal cord: Tg30, n=9 at 3 and 6 months of age and n=16 at 9 months of age respectively; 5xFAD x Tg30, n=7, 5, 12at 3, 6 and 9 months of age, respectively).

§§§, $p<0.0001$: significantly different from the same genotype at 3 months of age.

¤¤¤, $p<0.0001$: significantly different from the same genotype at 6 months of age.

&&&, $p<0.0001$: significantly different from Tg30 mice at the same age.

Figure 6

Higher level of Sarkosyl-insoluble tau proteins and of abnormal AD tau epitopes in 5xFAD x Tg30 mice compared to Tg30 mice

Western blotting and densitometry analysis of Sarkosyl-insoluble tau in brain of 9-month-old mice.

A) Representative Western blots with the B19 anti-tau antibody (total tau) and the BR21 human specific tau antibody (human tau) in wild-type (lane 1), 5xFAD (lane 2), Tg30 (lane 3) and 5xFAD x Tg30 (lane 4) mice. Sarkosyl-insoluble tau was detected only in Tg30 and 5xFAD xTg30 mice.

B) Densitometry quantification. The levels of insoluble total tau and of human tau were significantly higher in 5xFAD x Tg30 mice than in Tg30 mice. Levels of Sarkosyl-insoluble tau proteins were expressed as a percentage of the levels in Tg30 mice, taken as reference.

(***, $p<0.001$: by Student unpaired t-test), (Tg30, n=19 and 5xFAD x Tg30, n=10).

C) Representative Western blots with the phospho-tau antibodies AT100 and TG3, the conformation-dependent tau antibodies MC1 and Alz50 and the tau Asp421 antibody to caspase-cleaved Tau in Tg30 (lanes 1 and 2) and 5xFAD x Tg30 (lanes 3 and 4). The TG3, Alz50 and tauAsp421 epitopes are detected only in 5xFAD x Tg30 mice. AT100 and MC1 tau immunoreactivities are higher in 5xFAD x Tg30 mice.

D) Densitometry quantification. The level of MC1 immunoreactive insoluble tau, normalized to total tau, was higher in 5xFAD x Tg30 mice at 9 months of age than in Tg30 mice. Levels of MC1 insoluble tau/total tau ratios were expressed as a percentage of the levels in Tg30 mice.
(**, $p<0.01$: by Student unpaired t-test), (Tg30, n=12 and 5xFAD xTg30, n=15)
E) Densitometry quantification. The level of AT100 immunoreactive insoluble tau, normalized to total tau, was higher in 5xFAD x Tg30 mice at 9 months of age (n=4) than in Tg30 mice (n= 5). Levels of AT100 insoluble tau/total tau ratios were expressed as a percentage of the levels in Tg30 mice. (*, $p<0.05$: by Student unpaired t-test), (Tg30, n=5 and 5xFAD xTg30, n=4).

Figure 7

Increased phosphorylation of insoluble and soluble tau in brain of 5xFAD x Tg30 mice.

Western blotting analysis of phosphotau proteins in brain of 9-month-old Tg30 and 5xFAD x Tg30 mice

A) Representative Western blots with antibodies to pThr181 tau (AT270), to pSer202 tau (CP13), to pThr231/Thr235 tau (AT180), to pSer396/404 tau (PHF-1), and to total tau (B19) on brain Sarkosyl-insoluble fractions of Tg30 and 5xFAD x Tg30 mice. Phosphotau immunoreactivity was higher in 5xFAD x Tg30 mice. In addition to major 62-64 kDa Sarkosyl-insoluble tau protein present in both Tg30 and 5xFAD x Tg30 mice, phosphorylated tau species of higher molecular weight (arrows) or tau species of lower molecular weight (arrowheads) were also detected in 5xFAD x Tg30 mice.

B) Representative Western blots with antibodies to total tau (B19), to pThr181 tau (AT270), to pSer202 tau (CP13), to pThr231/Thr235 tau (AT180), to pSer396/404 tau (PHF-1) and to actin on brain soluble fractions of Tg30 and 5xFAD x Tg30 mice. A highly phosphorylated tau species with a slower electrophoretic mobility (arrows) was more abundant in 5xFAD x Tg30 mice.

C) Densitometry quantification. The degree of phosphorylation of Sarkosyl-insoluble tau (normalized to total insoluble tau) was significantly increased in 5xFAD x Tg30 compared to Tg30 mice. Levels of phosphorylated insoluble tau were expressed as a percentage of the levels in Tg30 mice. (*, $p<0.05$; **, $p<0.01$; ***, $p<0.0001$: by Student unpaired t-test), (Tg30, n=11 and 5xFAD x Tg30, n=10).

D) Densitometry quantification. The degree of phosphorylation of Sarkosyl-soluble tau (normalized to total soluble tau) was significantly increased for several epitopes in 5xFAD x Tg30 mice. Levels of phosphorylated soluble tau were expressed as a percentage of the levels in Tg30 mice. (*, $p<0.05$; **, $p<0.01$: by Student unpaired t-test), (Tg30, n=14; 5xFAD x Tg30, n=6).

Figure 8

Recruitment of murine tau into PHF in brain of 5xFAD x Tg30 mice.

Western blotting and ultrastructural immunolabelling analysis of murine tau proteins in 9-month-old Tg30 and 5xFAD x Tg30 mice

A) Western blots on brain Sarkosyl-insoluble fractions of Tg30 and 5xFAD x Tg30 mice with the murine specific tau antibody mTau5 and the B19 (total tau) antibody. Sarkosyl-insoluble murine tau was detected in brain of 5xFAD x Tg30 mice but not of Tg30 mice.

B) Ultrastructural immunolabelling of PHF present in Sarkosyl-insoluble brain fractions with the BR21 antibody to human tau (15 nm gold particles) and the mTau5 antibody to murine tau (5 nm gold particles). Murine tau was integrated with human tau into PHF from brain of 5xFAD x Tg30 mice but much less in PHF from brain of Tg30 mice. Scale bar: 250 nm.

Figure 9

Reduced amyloid deposition in brain and in spinal cord of 5xFAD x Tg30 mice.

Immunohistochemical analysis of Aß load in 5xFAD and 5xFAD x Tg30 mice.

A) Immunohistochemical labelling with anti-Aß40 and anti-Aß42 antibodies on sections of the cortex (panels 1-4) and of the spinal cord (panels 5-8) of 9-month-old 5xFAD and 5xFAD x Tg30 mice. The Aß40 and Aß42 deposits are smaller and less numerous in the cortex and the spinal cord of 5xFAD x Tg30 mice than in 5xFAD mice.

Scale bars = 100 µm. In 4, scale bar for panels 1, 2, 3 and 4. In 6, for panels 5 and 6. In 8, for panels, 7 and 8.

B - D) Quantification of the areas covered by Aβ40 and Aβ42 deposits in hippocampus (B), in cerebral cortex (C) and in gray matter of the spinal cord (D). Aß40 and Aß42 loads increase with age in both 5xFAD and 5xFAD xTg30 mice but are lower in 5xFAD x Tg30 mice, most markedly in the spinal cord. The statistical difference was evaluated by using a two-way Anova followed by a Bonferroni's Multiple Comparison Test (5xFAD: n=6 for hippocampus and cerebral cortex at 3, 6 and 9 months of age and 7, 8 and 10 mice at 3, 6 and 9 months of age for spinal cord; 5xFAD x Tg30: n=5 for hippocampus and cerebral cortex at 3 and 6 months of age, n= 10 at 9 months of age and for spinal cord, n=8, 5 and 12 at 3, 6 and 9 months of age).

**, $p<0.01$; ***, $p<0.001$: overall effect of the factor (age or genotype) or interaction between them.

#, $p<0.05$ and ##, $p<0.01$: significantly different from 5xFAD at the same age.

Figure 10

Decrease of APP ß-CTFs and of Aβ in brain and spinal cord homogenates of 9-month-old 5xFAD x Tg30 mice.

Western blotting analysis of Aß and ß-CTFs in brain and spinal cord homogenates of 9-month-old mice.

A and **B)** Western-blots with the 6E10 Aß antibody on brain (A) and spinal cord (B) homogenates. Aß and ß-CTFs are detected in 5xFAD and 5xFAD xTg30 mice. The Aß signal is very weak in spinal cord of 5xFAD xTg30 mice.

C and **D)** Densitometry quantification. The levels of β-CTFs and of Aß in the brain (C) and in the spinal cord (D) are significantly reduced in 5xFAD x Tg30 mice compared to 5xFAD mice. Data were normalized to the respective actin expression level. Levels of ß-CTFs and of Aß were expressed as a percentage of the levels in 5xFAD mice. (*, $p<0.05$ and ***, $p<0.0001$: by Student unpaired t-test), (brain: n=4 5xFAD and n=6 5xFAD x Tg30; spinal cord: n=7 5xFAD and n=9 5xFAD x Tg30).

Supplementary Figure 1

ELISA analysis of Aβ40 levels.

The levels of soluble (A and B) and insoluble (C and D) Aβ40 are reduced in brain (A and C) and spinal cord (B and D) homogenates of 5xFAD x Tg30 mice compared to 5xFAD at 6 months of age. Levels of Aß40 were expressed as a percentage of the levels in 5xFAD mice
(*, $p<0.05$, by Student unpaired t-test), (n=4 for each genotype).

Supplementary Figure 2

Decrease of phospho-Thr668 APP ß-CTFs in brain of 10-month-old 5xFAD x Tg30 mice.

Western blotting analysis of phospho-Thr668 APP and ß-CTFs in brain homogenates of 10-month-old 5xFAD and 5xFAD x Tg30 mice

A) Western-blots with the 2104 (anti-phospho-Thr668 APP) and 2061 (anti-APP) antibodies on brain homogenates detected phospho-Thr668 APP, phospho-Thr668 APP ß-CTFs and total APP in 5xFAD (lanes 1, 2) and 5xFAD xTg30 (lanes 3, 4) mice. The phospho-Thr668 APP ß-CTFs signal is reduced in brain of 5xFAD xTg30 mice.

B and C) Densitometry quantification. The levels of phosphorylated APP ß-CTFs (B) (nomalized to total APP) are significantly reduced in brain homogenates of 5xFAD x Tg30 mice compared to

5xFAD. The levels of phospho-Thr668 APP (C) are not significantly reduced. Levels of ß-CTFs and of of phospho-Thr668 APP were expressed as a percentage of the levels in 5xFAD mice.
(**, $p<0.01$: by Student unpaired t-test) (n=5 for 5xFAD and n=4 for 5xFAD x Tg30 mice).

Table 1: Primary antibodies used in this study

Antibody	Species	Epitope (cross-reactivity)	Source	Reference
B19	Rabbit polyclonal	bovine tau (human & mouse)	J.P. Brion	Brion, et al., 1991a
BR21	Rabbit polyclonal	amino acids 16-28 of human tau (human)	J.P. Brion	Ando, et al., 2011
BR10	Rabbit polyclonal	amino acids 84-101(insert 2) of human tau (human & mouse)	J.P. Brion	Hanger, et al., 2002
mTau5	Mouse monoclonal	mouse tau (mouse)	M. Mercken	Sennvik et al., 2007
AT8	Mouse monoclonal	phosphorylated tau at Ser202, Thr205 (human & mouse)	Innogenetics	Goedert et al., 1995
AT180	Mouse monoclonal	phosphorylated tau at Thr231 (human & mouse)	Innogenetics	Goedert et al., 1994
AT270	Mouse monoclonal	phosphorylated tau at Thr181 (human & mouse)	Innogenetics	Goedert et al., 1994
AT100	Mouse monoclonal	phosphorylated tau at Thr212, Ser214 (human & mouse)	Innogenetics	Hoffmann et al., 1997
Asp421	Mouse monoclonal	caspase-cleaved tau at Asp421 (human & mouse)	Millipore	
PHF-1	Mouse monoclonal	phosphorylated tau at Ser396, Ser404 (human & mouse)	P. Davies	Otvos et al., 1994
CP13	Mouse monoclonal	phosphorylated tau at Ser202, Thr205 (human & mouse)	P. Davies	Otvos et al., 1994
TG-3	Mouse monoclonal	conformation-dependent phosphoTau Thr231 (human & mouse)	P. Davies	Jicha et al., 1997b
Alz50	Mouse monoclonal	N-terminus and C-terminus of tau (human & mouse)	P. Davies	Jicha et al., 1997a
MC1	Mouse monoclonal	N-terminus and C-terminus of tau (human & mouse)	P. Davies	Jicha et al., 1997a
3H5	Mouse monoclonal	N-terminus of human APP (human)	J.N. Octave	Philippe et al., 1996
2061	Rabbit polyclonal	17 amino acids of C-terminus of APP (human & mouse)	N. Sergeant	Sergeant et al., 2002
2104	Rabbit polyclonal	pThr668 of APP (human & mouse)	N. Sergeant	Sergeant et al., 2002
6E10	Mouse monoclonal	amino acids 1-16 of human Aβ (human)	Millipore	
Aß42	Rabbit polyclonal	6 amino acids from the C-terminus of human Aβ42 (human)	Millipore	
Aß40	Rabbit polyclonal	amino acids 34-40 within the C-terminus region of human Aβ	BioSource	
PS1	Rat monoclonal	N-terminus of human PS-1 (amino acids 21-80) (human)	Chemicon	
SB129	Rabbit polyclonal	N-terminus of PS-1 (human & mouse)	C. Van Broeckhoven	Hendriks et al., 1998
ß-actin	Rabbit polyclonal	C-terminus of actin (mouse)	Sigma	
α-tubulin	Mouse monoclonal	Chicken brain microtubules (mouse)	Sigma	
GFAP	Mouse monoclonal	Pig GFAP (mouse)	Sigma	
Iba1	Goat polyclonal	amino acids 81-93 of human AIF-1 (mouse)	Abcam	

Table 2: Characteristics of transgenic lines

Transgenic line	Motor deficit	Hippocampal neuronal loss	NFT	Levels of insoluble tau	Misfolding of insoluble tau	Phosphorylation of insoluble tau	Truncation of insoluble tau	Phosphorylation of soluble tau	Insoluble murine tau	Amyloid pathology
Wild-type	-	-	-	-	-	-	-	+	-	-
5xFAD	-	-	-	-	-	-	-	+	-	+++
Tg30	++	-	++	++	+	++	-	++	+	-
5xFAD x Tg30	+++	+	+++	+++	++	+++	+	+++	++	++

Behavioral and brain pathological features of transgenic lines. - : absent ; + : moderate ; ++ : imortant ; +++ : very important

Fig 1

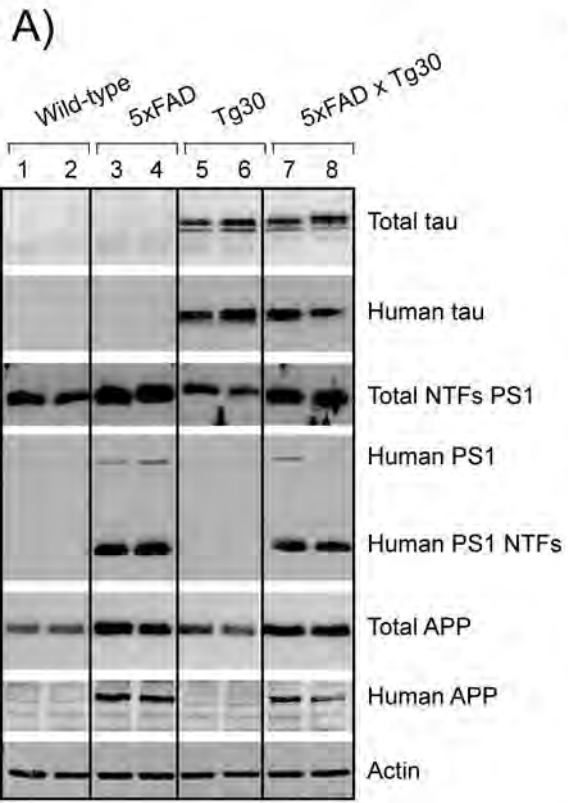
A)
Wild-type
5xFAD
Tg30
5xFAD x Tg30
1 2 3 4 5 6 7 8
Total tau
Human tau
Total NTFs PS1
Human PS1
Human PS1 NTFs
Total APP
Human APP
Actin

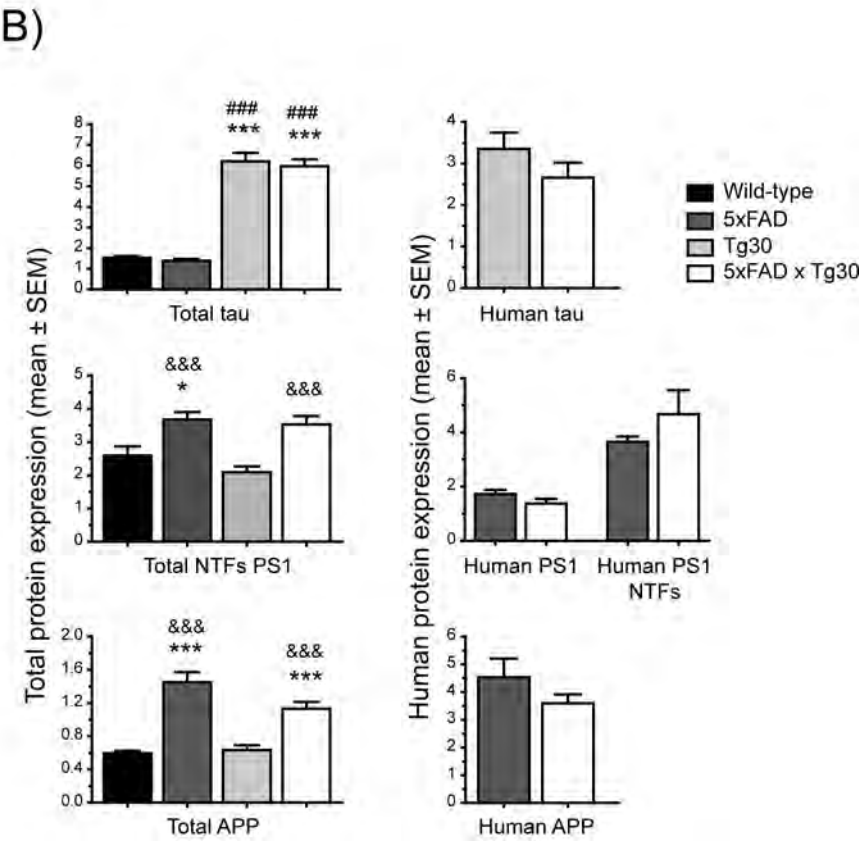
B)
Wild-type
5xFAD
Tg30
5xFAD x Tg30
Total protein expression (mean ± SEM)
Human protein expression (mean ± SEM)
Total tau
Human tau
Total NTFs PS1
Human PS1
Human PS1 NTFs
Total APP
Human APP
###
***
&&&
*

Fig 2

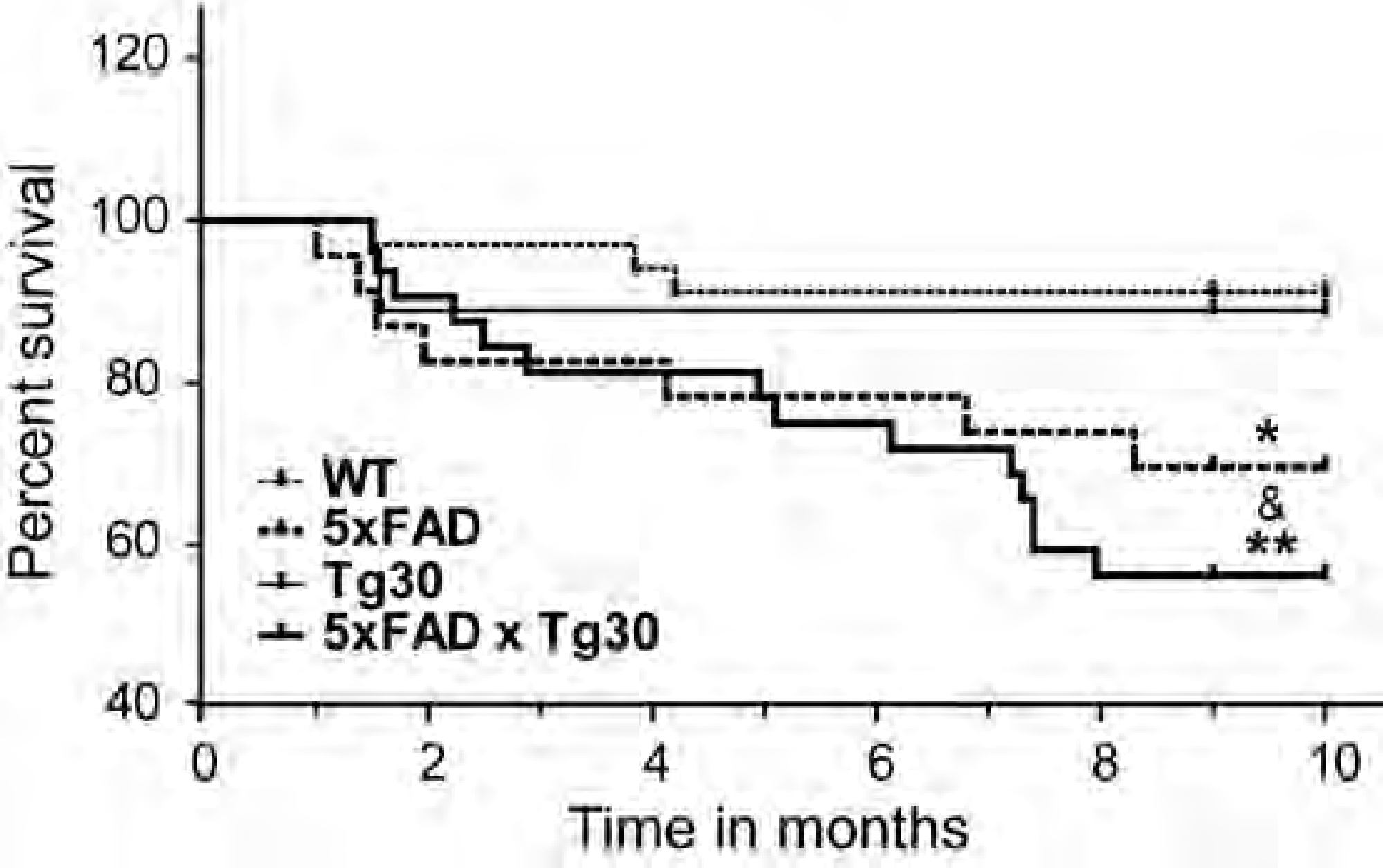
120
100
80
60
40
Percent survival
0
2
4
6
8
10
Time in months
WT
5xFAD
Tg30
5xFAD x Tg30
*
&
**

Fig 3

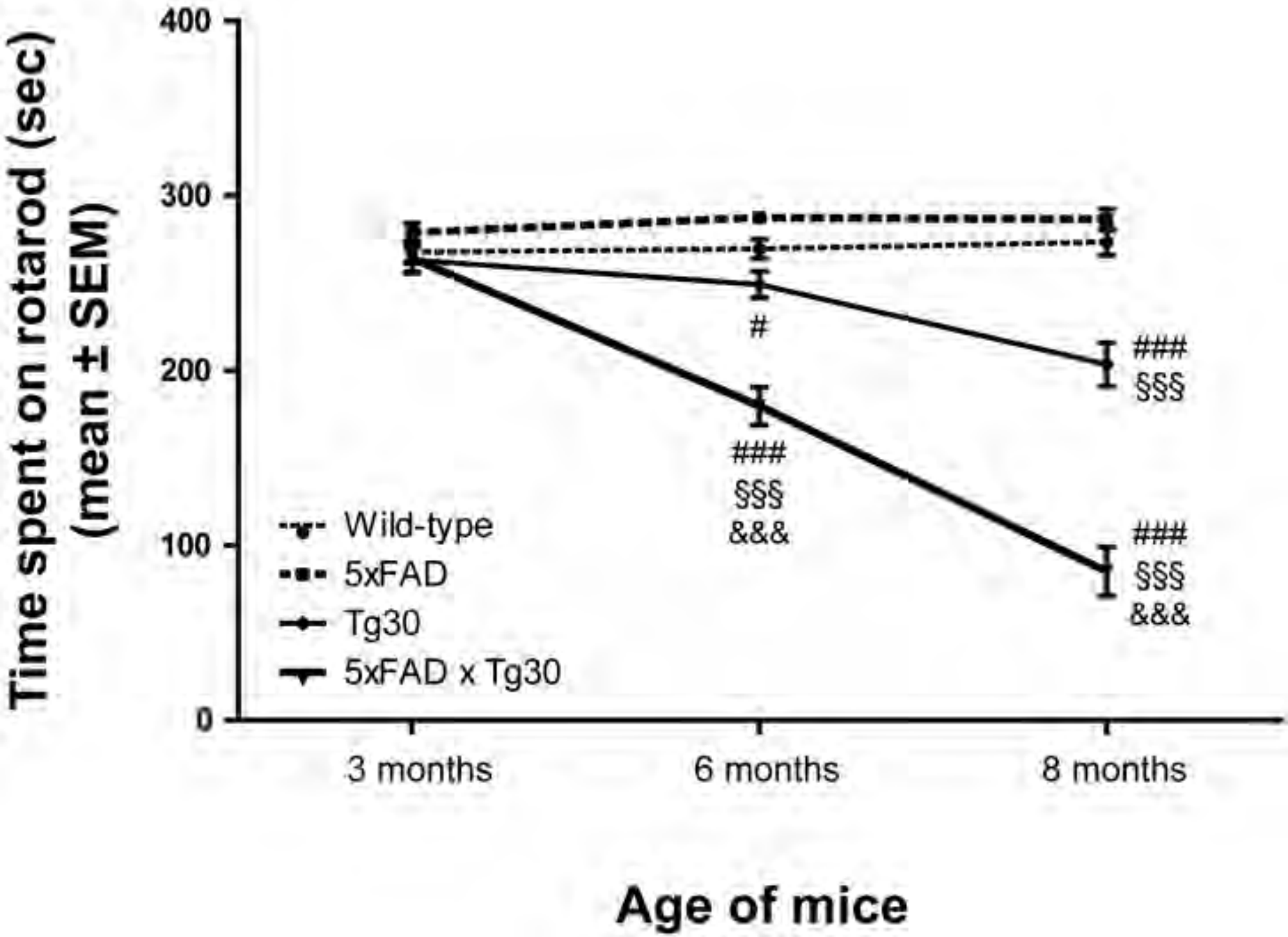

Age of mice

Fig 4

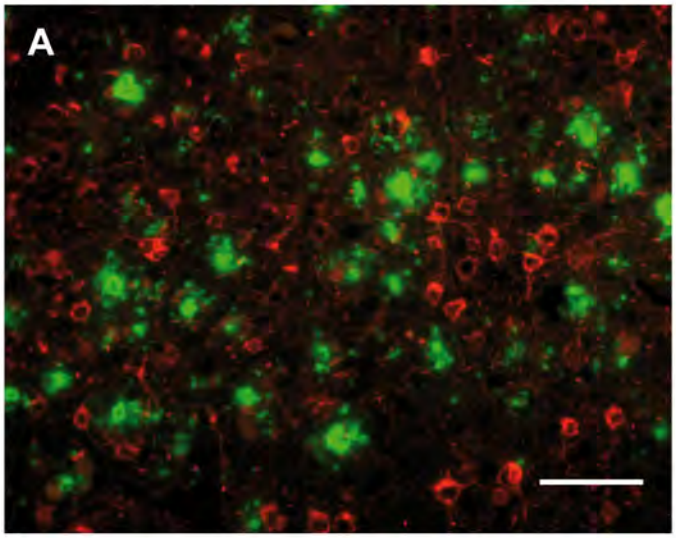

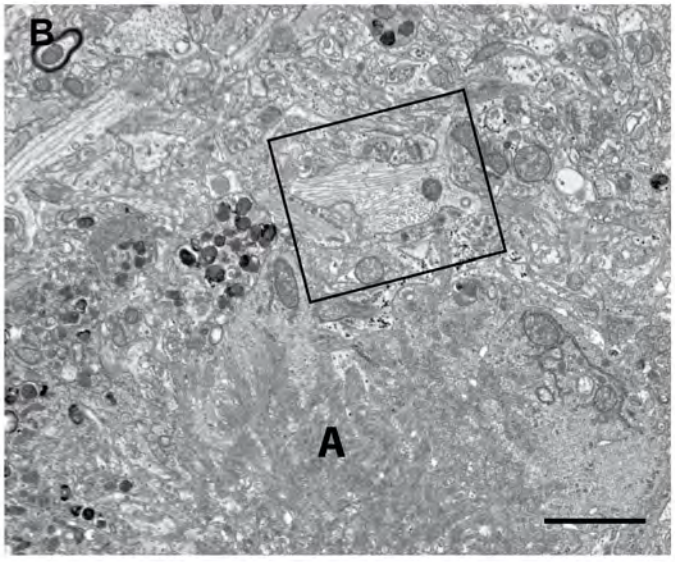

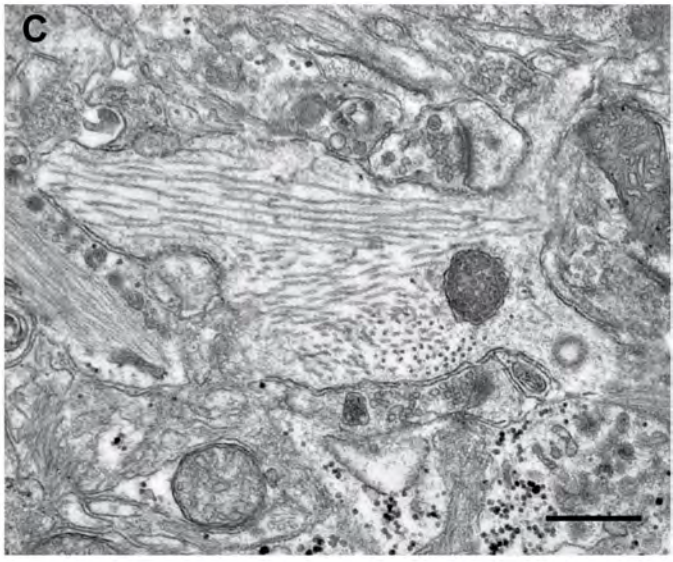

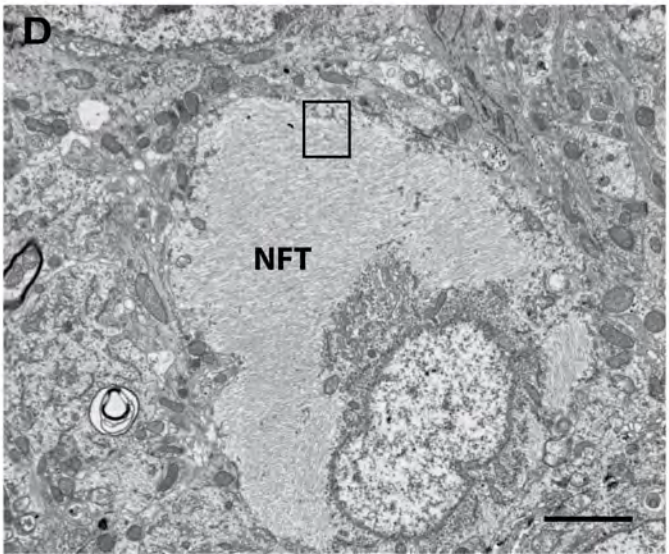

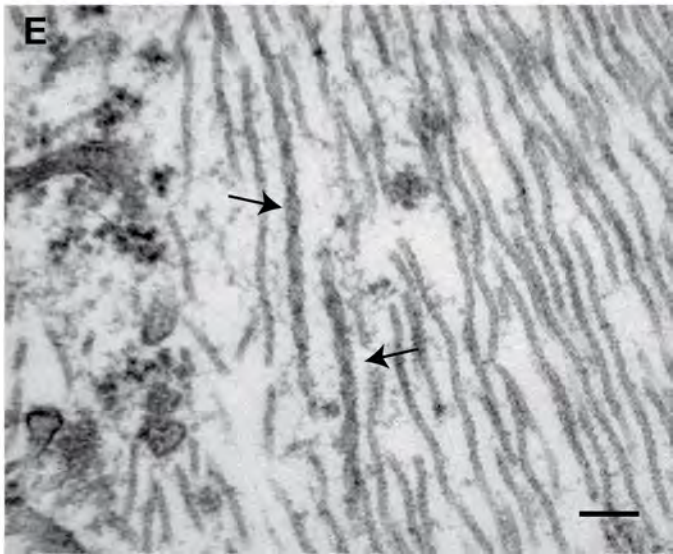

Fig 5

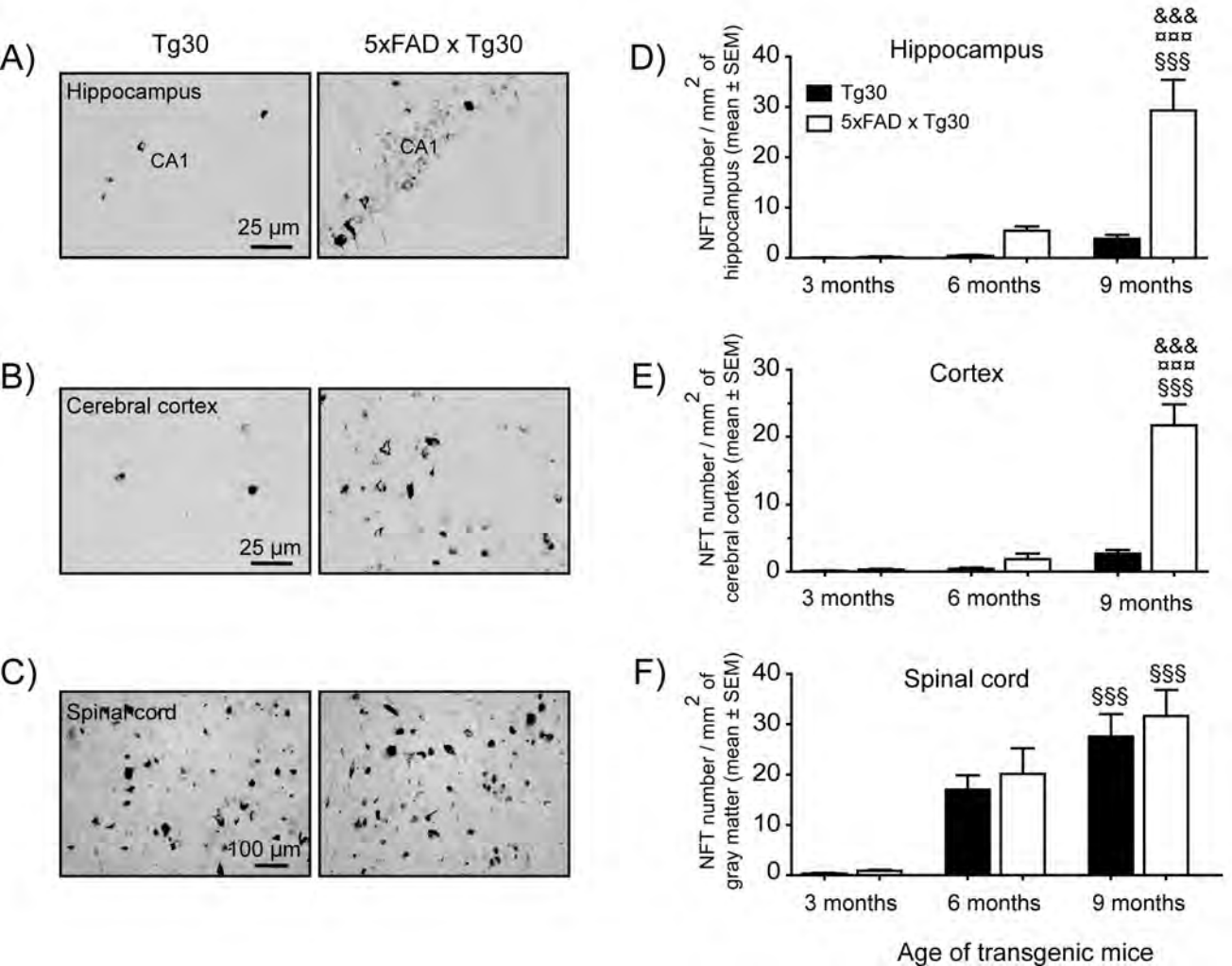
A)
Tg30
5xFAD x Tg30
Hippocampus
CA1
CA1
25 µm
B)
Cerebral cortex
25 µm
C)
Spinal cord
100 µm
D)
Hippocampus
Tg30
5xFAD x Tg30
NFT number / mm 2 of hippocampus (mean ± SEM)
40
30
20
10
0
3 months
6 months
9 months
&&&
¤¤¤
§§§
E)
Cortex
NFT number / mm 2 of cerebral cortex (mean ± SEM)
30
20
10
0
3 months
6 months
9 months
&&&
¤¤¤
§§§
F)
Spinal cord
NFT number / mm 2 of gray matter (mean ± SEM)
40
30
20
10
0
3 months
6 months
9 months
§§§
§§§
Age of transgenic mice

Fig 6

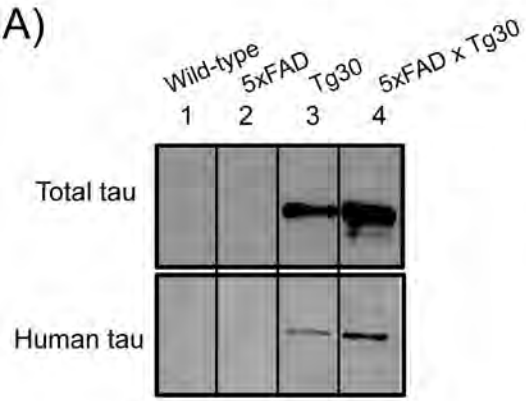
A)
Wild-type
5xFAD
Tg30
5xFAD x Tg30
1
2
3
4
Total tau
Human tau

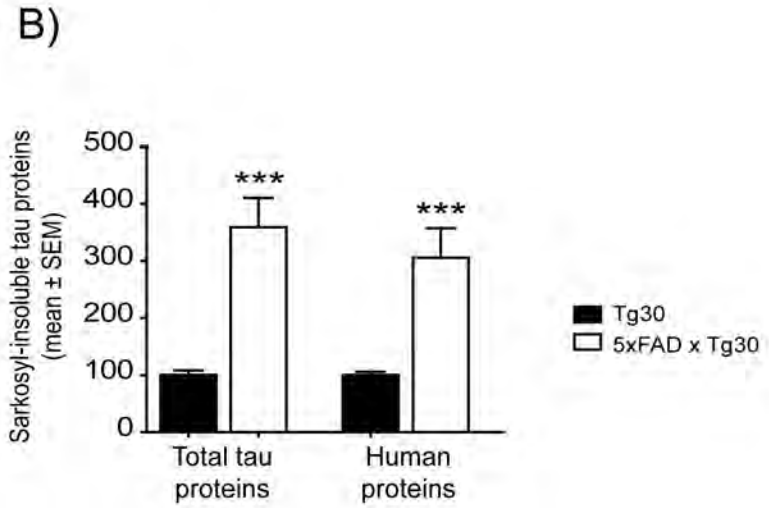
B)
Sarkosyl-insoluble tau proteins (mean ± SEM)
500
400
300
200
100
0
***
***
Total tau proteins
Human proteins
Tg30
5xFAD x Tg30

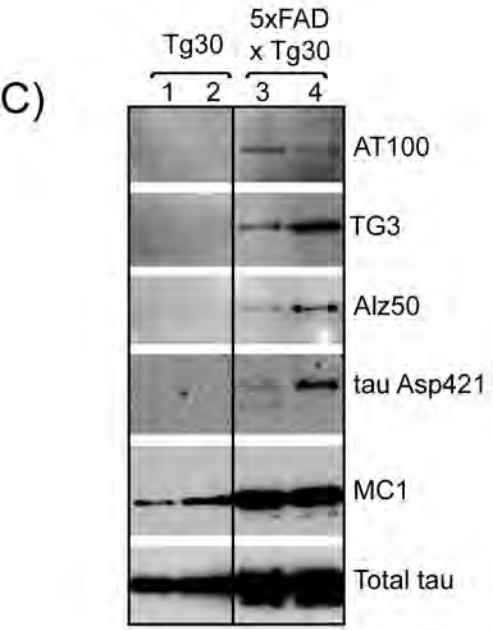
C)
Tg30
5xFAD x Tg30
1
2
3
4
AT100
TG3
Alz50
tau Asp421
MC1
Total tau

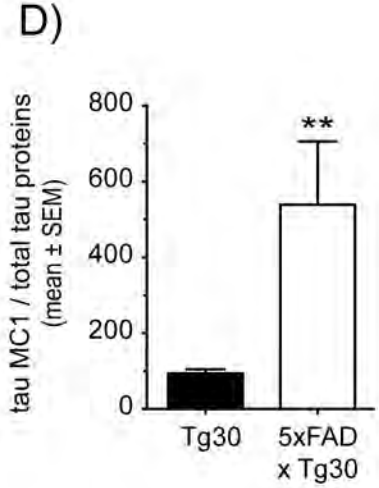
D)
tau MC1 / total tau proteins (mean ± SEM)
800
600
400
200
0
**
Tg30
5xFAD x Tg30

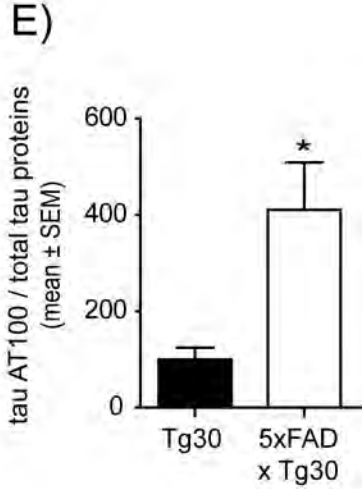
E)
tau AT100 / total tau proteins (mean ± SEM)
600
400
200
0
*
Tg30
5xFAD x Tg30

Fig 7

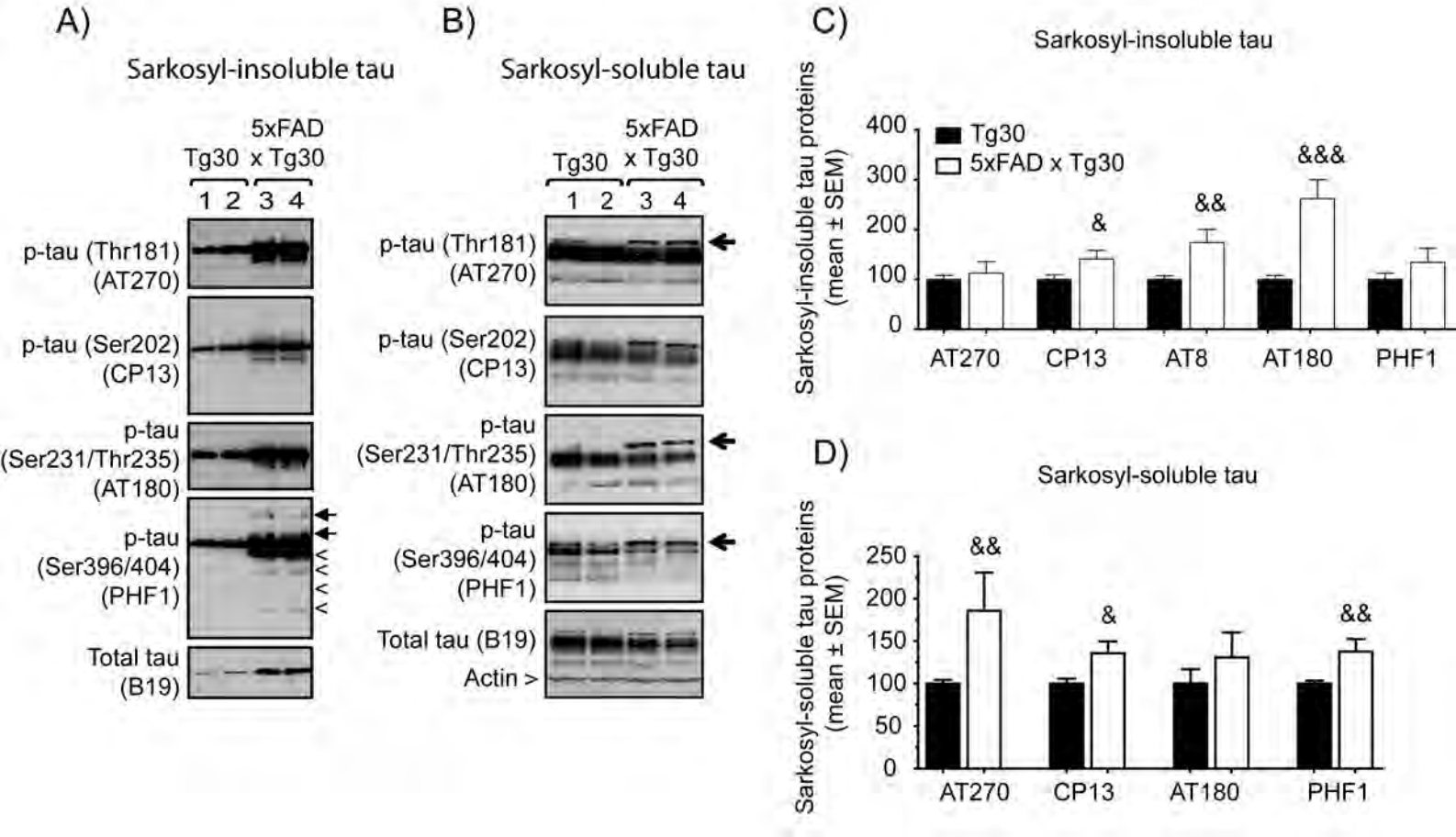
A)
Sarkosyl-insoluble tau
Tg30
5xFAD x Tg30
1 2 3 4
p-tau (Thr181) (AT270)
p-tau (Ser202) (CP13)
p-tau (Ser231/Thr235) (AT180)
p-tau (Ser396/404) (PHF1)
Total tau (B19)
B)
Sarkosyl-soluble tau
Tg30
5xFAD x Tg30
1 2 3 4
p-tau (Thr181) (AT270)
p-tau (Ser202) (CP13)
p-tau (Ser231/Thr235) (AT180)
p-tau (Ser396/404) (PHF1)
Total tau (B19)
Actin >
C)
Sarkosyl-insoluble tau
Sarkosyl-insoluble tau proteins (mean ± SEM)
Tg30
5xFAD x Tg30
400
300
200
100
0
&
&&
&&&
AT270
CP13
AT8
AT180
PHF1
D)
Sarkosyl-soluble tau
Sarkosyl-soluble tau proteins (mean ± SEM)
250
200
150
100
50
0
&&
&
&&
AT270
CP13
AT180
PHF1

Fig 8

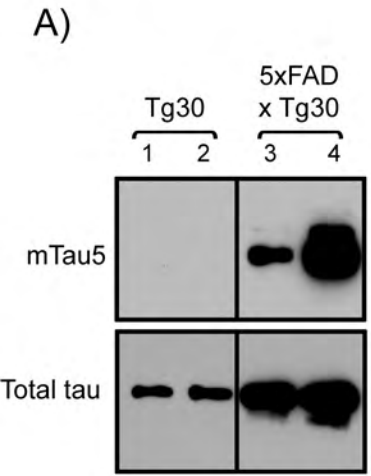

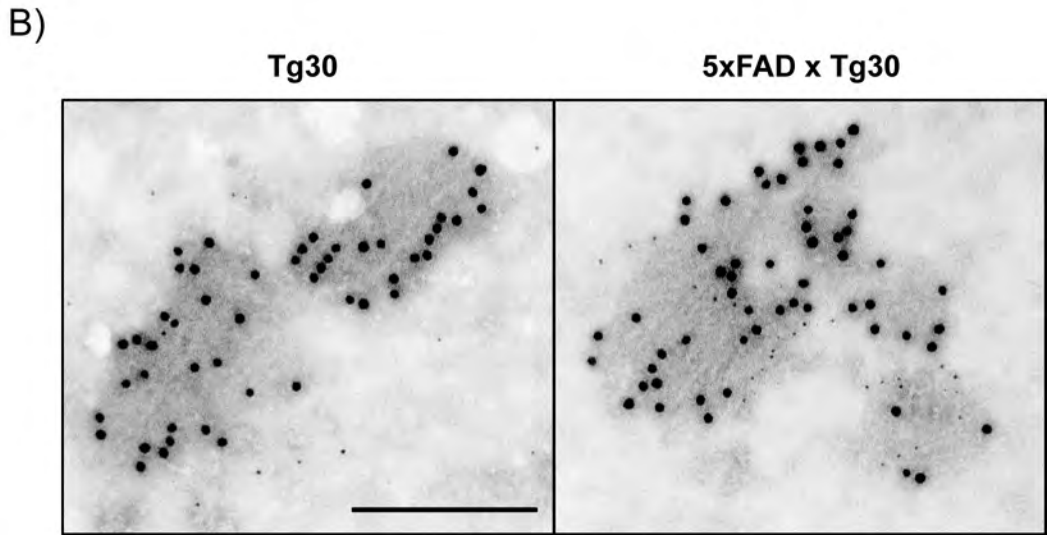

Fig 9

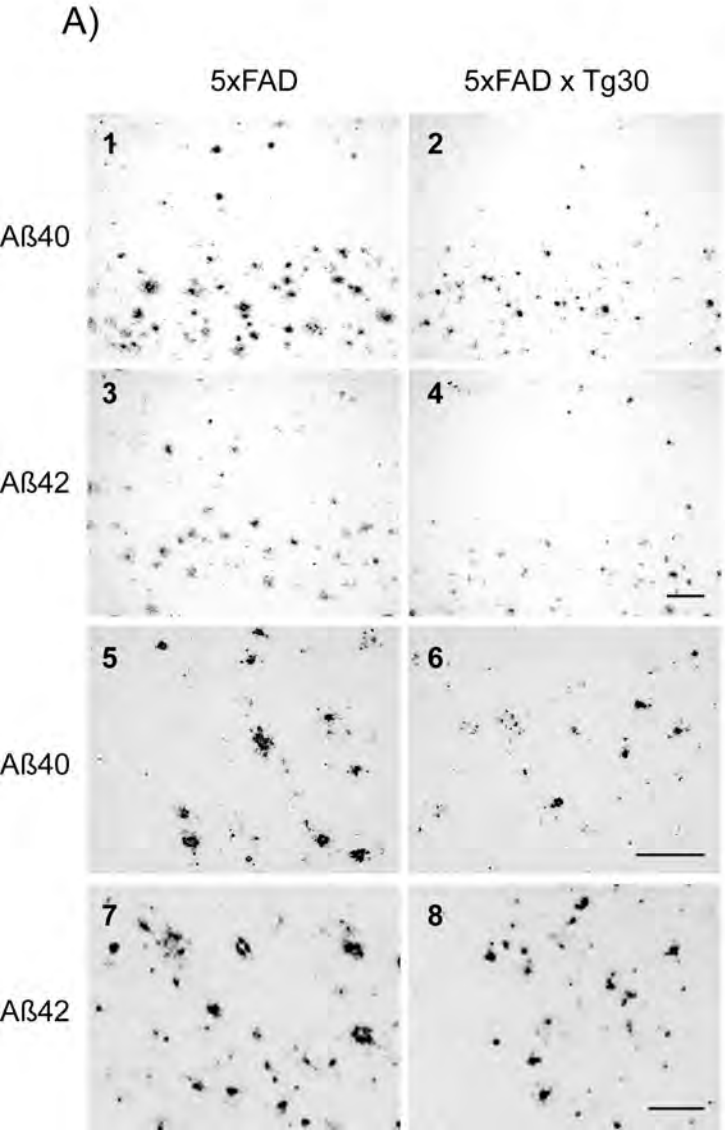
A)
5xFAD
5xFAD x Tg30
Aß40
Aß42
Aß40
Aß42
1
2
3
4
5
6
7
8

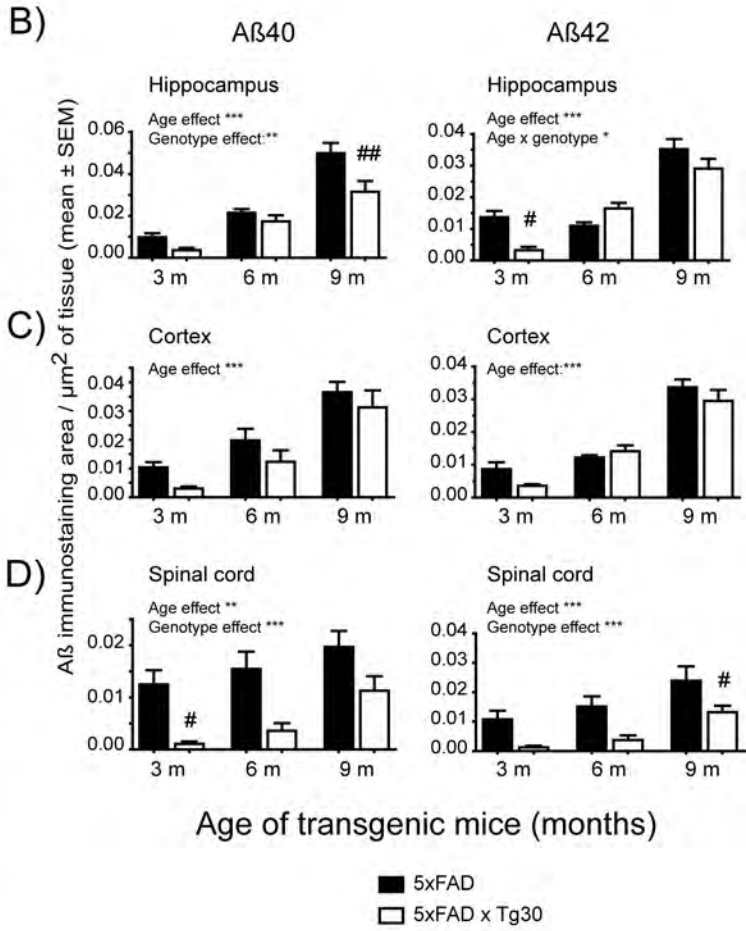
B)
Aß40
Aß42
Hippocampus
Age effect ***
Genotype effect:**
Hippocampus
Age effect ***
Age x genotype *
C)
Cortex
Age effect ***
Cortex
Age effect:***
D)
Spinal cord
Age effect **
Genotype effect ***
Spinal cord
Age effect ***
Genotype effect ***
Aß immunostaining area / µm2 of tissue (mean ± SEM)
3 m
6 m
9 m
Age of transgenic mice (months)
5xFAD
5xFAD x Tg30

Fig 10

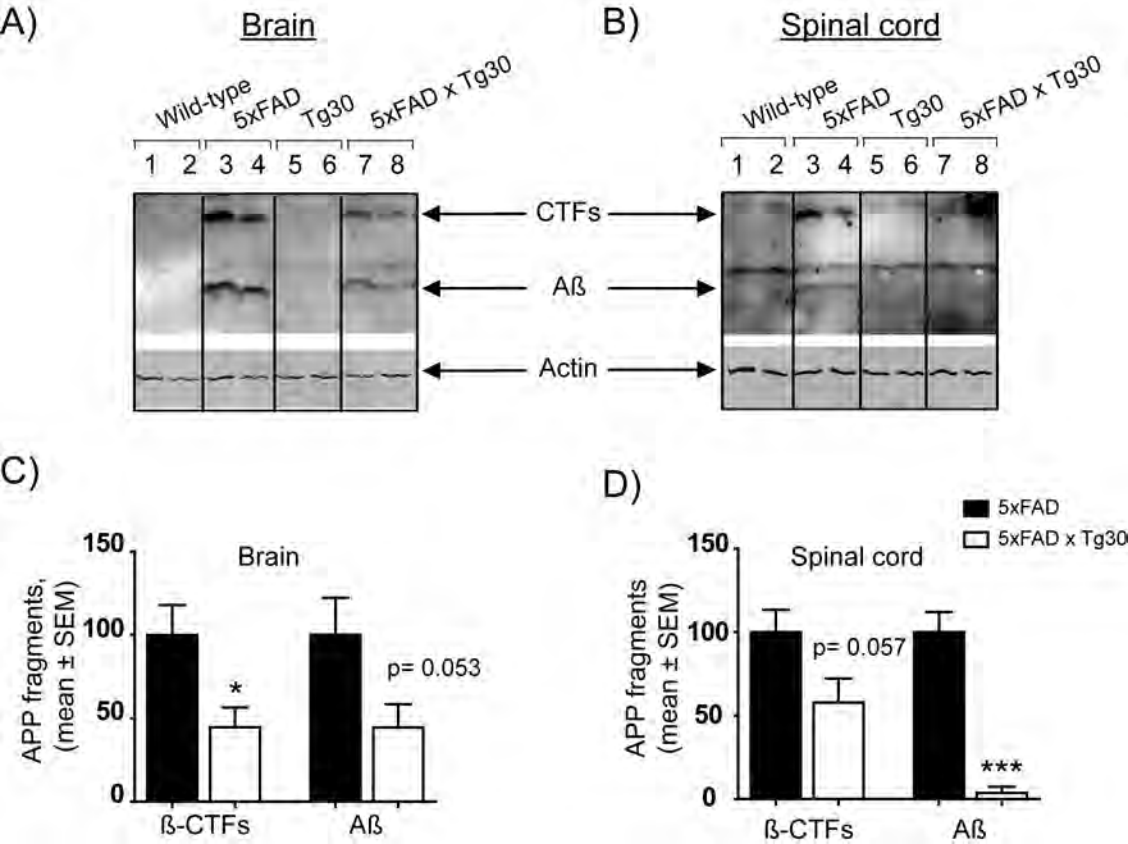
A)
Brain
B)
Spinal cord
Wild-type
5xFAD
Tg30
5xFAD x Tg30
1 2 3 4 5 6 7 8
CTFs
Aß
Actin
C)
Brain
APP fragments, (mean ± SEM)
150
100
50
0
*
p= 0.053
ß-CTFs
Aß
D)
5xFAD
5xFAD x Tg30
Spinal cord
p= 0.057
***

Supplementary Fig 1

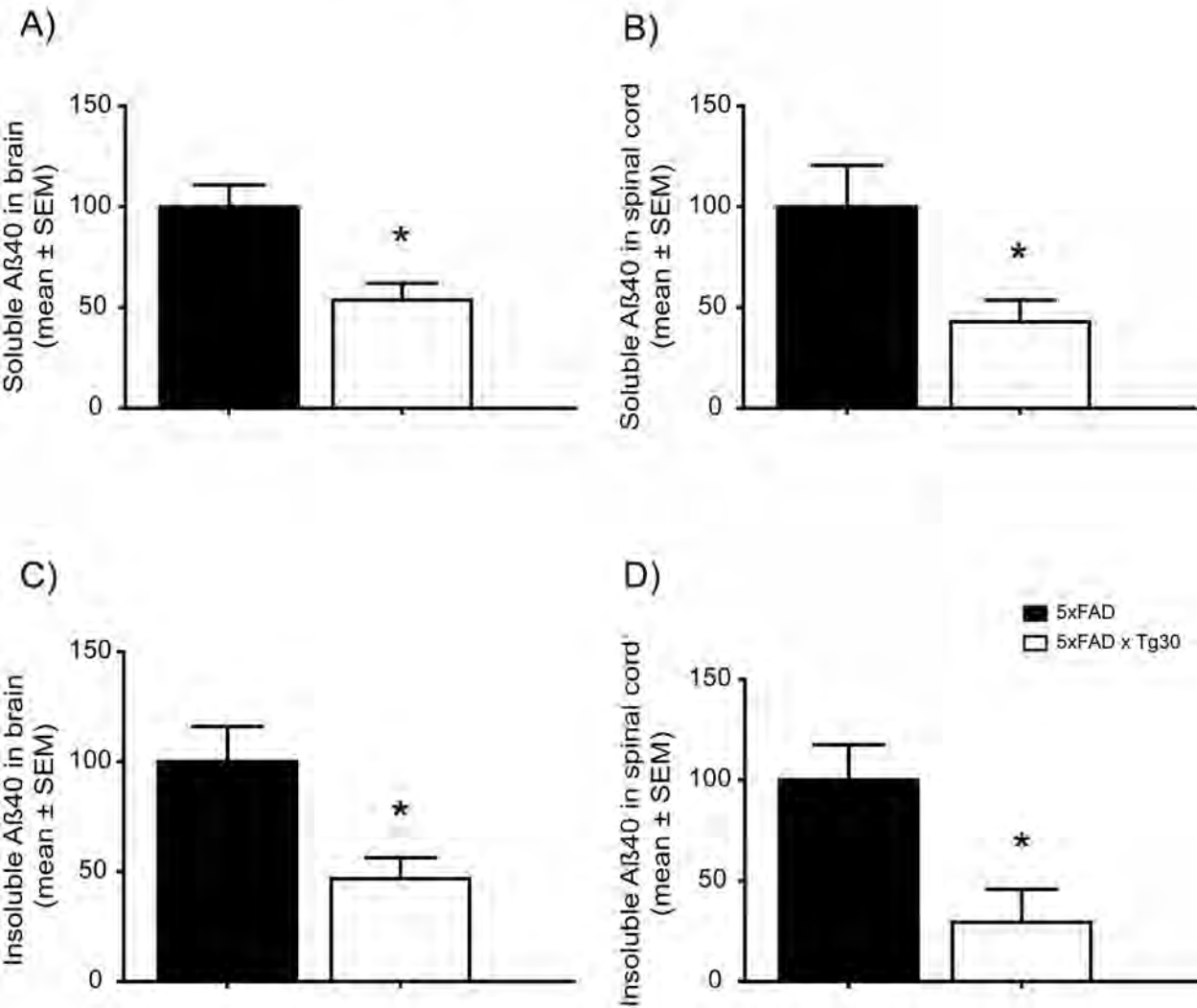

Supplementary Fig 2